Composite synoptic-scale environments conducive to North American polar–subtropical jet superposition events

By

ANDREW C. WINTERS[1*], DANIEL KEYSER[2], LANCE F. BOSART[2], and JONATHAN E. MARTIN[3]

[1]Department of Atmospheric and Oceanic Sciences
University of Colorado Boulder
Boulder, CO 80309

[2]Department of Atmospheric and Environmental Sciences
University at Albany, State University of New York
Albany, NY 12222

[3]Department of Atmospheric and Oceanic Sciences
University of Wisconsin–Madison
Madison, WI 53706

Submitted for publication in *Monthly Weather Review*
23 October 2019

Revised version submitted
24 January 2020

[*] *Corresponding author address:* Andrew C. Winters, Dept. of Atmospheric and Oceanic Sciences, University of Colorado Boulder, 311 UCB, Boulder, CO 80309. E-mail: andrew.c.winters@colorado.edu

ABSTRACT

A polar–subtropical jet superposition represents a dynamical and thermodynamic environment conducive to the production of high-impact weather. Prior work indicates that the synoptic-scale environments that support the development of North American jet superpositions vary depending on the case under consideration. This variability motivates an analysis of the range of synoptic-dynamic mechanisms that operate within a double-jet environment to produce North American jet superpositions. This study identifies North American jet superposition events during November–March 1979–2010 and subsequently classifies those events into three characteristic event types. "Polar dominant" events are those during which only the polar jet is characterized by a substantial excursion from its climatological latitude band, "subtropical dominant" events are those during which only the subtropical jet is characterized by a substantial excursion from its climatological latitude band, and "hybrid" events are those characterized by a mutual excursion of both jets from their respective climatological latitude bands. The analysis indicates that North American jet superposition events occur most often during November and December, and that subtropical dominant events are the most frequent event type for all months considered. Composite analyses constructed for each event type reveal the consistent role that descent plays in restructuring the tropopause beneath the jet-entrance region prior to jet superposition. The composite analyses further show that surface cyclogenesis and widespread precipitation lead the development of subtropical dominant events and contribute to jet superposition via their associated divergent circulations and diabatic heating, whereas surface cyclogenesis and widespread precipitation tend to peak at the time of superposition and well downstream of polar dominant events.

1. Introduction

The instantaneous positions of the polar and subtropical jets are closely related to the pole-to-equator tropopause structure, as indicated by the idealized vertical cross section in Fig. 1a. In the Northern Hemisphere, the average location of the polar jet is near 50°N in the region where the tropopause height abruptly rises from the polar tropopause (~350 hPa) to the subtropical tropopause (~250 hPa). The polar jet also resides atop the strongly baroclinic and tropospheric-deep polar front (e.g., Palmén and Newton 1948; Namias and Clapp 1949; Newton 1954; Palmén and Newton 1969, Keyser and Shapiro 1986; Shapiro and Keyser 1990). The average position of the subtropical jet is located equatorward of the polar jet near 30°N in the region where the tropopause height abruptly rises from the subtropical tropopause (~250 hPa) to the tropical tropopause (~100 hPa). In contrast to the polar jet, the subtropical jet is characterized by relatively modest baroclinicity in the upper troposphere and lower stratosphere (e.g., Starr 1948; Loewe and Radok 1950; Yeh 1950; Koteswaram 1953; Mohri 1953; Koteswaram and Parthasarathy 1954; Sutcliffe and Bannon 1954; Krishnamurti 1961; Riehl 1962).

Although the polar and subtropical jets typically occupy separate climatological latitude bands, the latitudinal separation between the two jets occasionally vanishes, resulting in a polar–subtropical jet superposition (e.g., Winters and Martin 2014, 2016, 2017; Handlos and Martin 2016; Christenson et al. 2017). An idealized vertical cross section perpendicular to the axis of a jet superposition is shown in Fig. 1b and reveals the principal characteristics of a superposition. These characteristics include the development of (1) a steep, single-step pole-to-equator tropopause structure, (2) anomalously strong wind speeds that can exceed 100 m s^{-1} in some instances, and (3) strong baroclinicity in the upper troposphere and lower stratosphere. The development of strong baroclinicity in association with the jet superposition is also accompanied by the formation of a vigorous across-front ageostrophic circulation that can directly influence the production of high-impact weather (e.g., Winters and Martin 2014, 2016, 2017).

A climatology of Northern Hemisphere jet superpositions using the NCEP–NCAR Reanalysis dataset (Kalnay et al. 1996; Kistler et al. 2001) during November–March 1960–2010 indicates that jet superpositions are most frequent over the western North Pacific, North America, and northern Africa (Christenson et al. 2017). The key dynamical processes associated with western North Pacific jet superpositions have been examined in detail by Handlos and Martin (2016). These dynamical processes include equatorward surges of lower-tropospheric cold air over the east Asian continent that act to strengthen the lower-tropospheric baroclinicity at middle and subtropical latitudes, and the development of widespread convection over the equatorial western North Pacific.

Prior work concerning North American jet superpositions has focused solely on individual case studies. Winters and Martin (2014, 2016) examined the development of a jet superposition during the 1–3 May 2010 Tennessee Flood, and determined that a substantial fraction of the poleward moisture transport into the southeastern U.S. prior to the second day of the event was attributable to the across-front ageostrophic circulation associated with the superposed jet. This poleward moisture transport ensured that widespread precipitation continued throughout the second day of the event (Moore et al. 2012). Furthermore, the presence of widespread precipitation during the May 2010 Tennessee Flood contributed to the diabatic erosion of upper-tropospheric potential vorticity (PV) on the equatorward side of the subtropical jet and strong negative PV advection by the irrotational wind along the axis of the subtropical jet. These two processes facilitated a poleward shift in the position of the subtropical waveguide and the formation of the steep, single-step tropopause structure that accompanied the jet superposition.

Winters and Martin (2016, 2017) performed a complementary analysis of a wintertime jet superposition event on 20 December 2009 that featured a rapidly deepening surface cyclone beneath the poleward-exit region of the superposed jet. This cyclone was associated with snowfall in excess of 30 cm (~12 in.) in locations ranging from the Mid-Atlantic northeastward towards New England. In contrast to the May 2010 Tennessee Flood, widespread precipitation on the equatorward side of the subtropical jet did not contribute substantially to the development of a single-step tropopause structure during the December 2009 case. Instead, Winters and Martin (2016, 2017) determined that the descending branch of an across-front ageostrophic circulation within the double-jet environment acted to restructure the tropopause prior to superposition.

The two aforementioned cases served as the foundation for the conceptual model of North American jet superpositions (Fig. 1c) introduced by Winters and Martin (2017; their Fig. 2). In this model, jet superposition features the development of a polar cyclonic PV anomaly at high latitudes with a polar jet located equatorward of the PV anomaly. Polar cyclonic PV anomalies, which include coherent tropopause disturbances (e.g., Hakim 2000; Pyle et al. 2004) and tropopause polar vortices (e.g., Cavallo and Hakim 2009, 2010, 2012, 2013), typify a dynamical environment that can be conducive to surface cyclogenesis at middle and high latitudes (e.g., Hakim et al. 1995, 1996; Pyle et al. 2004; Cavallo and Hakim 2010).

Jet superposition also features the concomitant production of a tropical anticyclonic PV anomaly on the equatorward side of the subtropical jet. Tropical anticyclonic PV anomalies result from the poleward transport of tropical, low-PV upper-tropospheric air via low-latitude troughs and tropical plumes (e.g., Iskenderian 1995; Roundy et al. 2010; Fröhlich et al. 2013; Winters and Martin 2016), and/or tropical cyclones (e.g., McTaggart-Cowan et al. 2007; Archambault et al. 2013, 2015). Tropical anticyclonic PV anomalies at middle latitudes typify a thermodynamic environment characterized by low upper-tropospheric static stability, and can contribute to the development of an atmospheric river (e.g., Newell et al. 1992; Zhu and Newell 1998; Ralph et al. 2004, 2018, 2019) within the poleward-directed branch of the tropospheric-deep, nondivergent circulation induced by the anticyclonic PV anomaly.

If polar cyclonic and tropical anticyclonic PV anomalies are situated within a confluent large-scale flow pattern and phase favorably, the result is a meridional juxtaposition of the respective PV anomalies at middle latitudes. This configuration encourages the superposition of the nondivergent circulations induced by each PV anomaly and a rapid increase in wind speed in the area between the two anomalies (e.g., Martin 2006b, p. 305). The meridional juxtaposition of the respective PV anomalies also establishes a dynamical and thermodynamic environment conducive to high-impact weather.

Once the respective PV anomalies are meridionally juxtaposed, mesoscale processes within the near-jet environment act to restructure the tropopause to produce the steep, single-step tropopause structure that accompanies a jet superposition (i.e., Fig. 1b). As demonstrated in the aforementioned case studies, mesoscale processes capable of restructuring the tropopause within a double-jet environment include across-front ageostrophic circulations (e.g., Shapiro 1981, 1982; Keyser and Pecnick 1985; Keyser and Shapiro 1986; Lang and Martin 2012; Martin 2014; Handlos and Martin 2016; Winters and Martin, 2016, 2017), as well as the diabatic heating and negative PV advection at the level of the dynamic tropopause by the irrotational wind that accompany areas of widespread precipitation (e.g., Lee and Kim 2003; Agustí-Panareda et al.

2004; Ahmadi-Givi et al. 2004; Son and Lee 2005; Grams et al. 2011, 2013; Archambault et al. 2013, 2015; Lang and Martin 2013b; Grams and Archambault 2016; Handlos and Martin 2016; Winters and Martin 2016, 2017).

Although the conceptual model presented in Fig. 1c generalizes the process of jet superposition over North America, it does not reveal the degree to which the dynamical processes responsible for producing a jet superposition (i.e., across-front ageostrophic circulations, diabatic heating, and negative PV advection at the level of the dynamic tropopause by the irrotational wind) vary between jet superposition events (e.g., Winters and Martin 2016; 2017). Furthermore, the conceptual model in Fig. 1c does not portray the spectrum of interactions that can occur between polar cyclonic and tropical anticyclonic PV anomalies prior to jet superposition. For instance, an individual jet superposition can arise solely in response to a substantial equatorward deviation of the polar jet towards the latitude of the subtropical jet, and vice versa. To address these shortcomings, this study characterizes the variability of North American jet superpositions, and reveals the spectrum of dynamical processes and synoptic-scale evolutions that lead to North American jet superpositions.

The remainder of this study is structured as follows. Section 2 introduces the automated identification scheme used to identify jet superposition events and the classification scheme employed to partition jet superposition events into event types. Section 3 discusses the climatological characteristics of each jet superposition event type. Section 4 discusses the composite synoptic-scale flow evolutions associated with selected jet superposition event types, and section 5 summarizes the results.

2. Data and methodology

This study employs data from the National Centers for Environmental Prediction Climate Forecast System Reanalysis (CFSR; Saha et al. 2010) with 0.5° grid spacing at 6-h intervals during November–March 1979–2010. This period ensures that the forthcoming analysis comprises a subset of the November–March 1960–2010 period examined by Christenson et al. (2017) and is consistent with the results from that study. The CFSR is chosen to better resolve the dynamical evolutions that precede jet superpositions than the coarser NCEP–NCAR reanalysis dataset (2.5° grid spacing) used in prior examinations of superpositions (e.g., Handlos and Martin 2016; Christenson et al. 2017). All CFSR data were bilinearly interpolated from isobaric surfaces onto isentropic surfaces between 300 K and 380 K at 5-K intervals to accommodate the forthcoming jet superposition identification scheme. This study also utilizes the NOAA Interpolated Outgoing Longwave Radiation (OLR) dataset (Liebmann and Smith 1996) with 2.5° grid spacing to construct daily composites of OLR for each jet superposition event type. Areas characterized by negative OLR anomalies serve as proxies for the location of extensive cloud cover, and may imply the presence of precipitation if the OLR anomalies overlap with a favorable dynamical and thermodynamic environment for synoptic-scale ascent.

a) Jet superposition event identification

The automated jet superposition identification scheme is identical to that described in Winters and Martin (2014, 2016), Handlos and Martin (2016), and Christenson et al. (2017). The scheme is grid-column based, in that it identifies grid columns that exhibit the characteristics of a polar jet and/or a subtropical jet. A polar jet or a subtropical jet is identified at a grid column if two criteria are satisfied. First, the integrated wind speed within that grid column must exceed 30 m s^{-1} within the 400–100-hPa layer. Second, the magnitude of the horizontal PV gradient within the 1–3-PVU channel at that grid column must exceed an empirically defined threshold[1] in the 315–330-K layer to identify a polar jet and in the 340–355-K layer to identify a subtropical jet. As implied by Fig. 1a, a strong horizontal PV gradient within the 1–3-PVU channel in the 315–330-K layer corresponds to a vertically oriented tropopause between the polar and subtropical tropopauses, and a strong PV gradient in the 340–355-K layer corresponds to a vertically oriented tropopause between the subtropical and tropical tropopauses. The identification of a polar and a subtropical jet within the same grid column at a single analysis time results in the identification of a jet superposition at that grid column, and is interpreted as the formation of a steep, single-step tropopause structure (i.e., Fig. 1b). On a horizontal map, this identification scheme is manifested at a single analysis time as a ribbon of positively identified grid columns that parallel the axis of a superposed jet (not shown).

North American jet superpositions were identified during the cold season (November–March) within the domain 10° to 80°N and 140° to 50°W. Although jet superpositions do occur outside of the cold season (e.g., the May 2010 Tennessee Flood), the aforementioned jet identification scheme would need to be modified to account for the seasonal variability of the isentropic layers that house the polar and subtropical jets in order to identify jet superpositions outside of the cold season.

Following their identification, all 6-h analysis times characterized by a jet superposition were filtered to retain only those times that rank in the top 10% in terms of the number of grid columns characterized by a jet superposition (i.e., those analysis times that featured 18 or more grid columns characterized by a superposition). This filter retains only those analysis times in which the polar and subtropical jets are vertically superposed along a substantial length of the jet

[1] The thresholds used for the magnitude of the horizontal PV gradient are 1.4×10^{-5} PVU m^{-1} within the 315–330-K layer and 0.9×10^{-5} PVU m^{-1} within the 340–355-K layer, where 1 PVU = 10^{-6} K m^{2} kg^{-1} s^{-1}.

axis. All grid columns characterized by a jet superposition during a retained analysis time were also required to be located within 1000 km of another grid column characterized by a superposition. If an analysis time featured a group of 18 or more grid columns that satisfied this distance criterion, it was labeled a "jet superposition event." Although rare, this filter allows for the identification of multiple jet superposition events at a single analysis time, so long as the groups of jet superposition grid columns are more than 1000 km apart and each group is at least 18 grid columns in size.

The latitude and longitude of each grid column associated with a single jet superposition event were averaged to compute a latitude–longitude centroid for that particular event. The positions of the jet superposition event centroids were then compared across all events to group together jet superposition events associated with the same jet. In particular, if an event centroid during one event was located within 1500 km of the location of another event centroid during the previous 30-h period[2], those jet superposition events were considered to be the same event. The methodology described within this section produced a total of 326 jet superposition events.

b) Jet superposition event classification

Following their identification, jet superposition events were classified into event types based on the degree to which the polar and subtropical jets deviated from their respective climatological positions to form a jet superposition. The climatological position of the polar waveguide at a single analysis time (e.g., 0000 UTC 1 January) was calculated by averaging the position of the 2-PVU contour on the 320-K surface at 24-h intervals within a 21-day window centered on that analysis time for every year between 1979 and 2010. The climatological

[2] The spatial thresholds used to identify jet superposition events approximately correspond to the Rossby radius of deformation for synoptic-scale features at midlatitudes (~1000–1500 km), and the temporal threshold corresponds to nearly double the average duration of a North American jet superposition event (~16 h).

position of the subtropical waveguide was similarly calculated by averaging the position of the 2-PVU contour on the 350-K surface. The 320- and 350-K surfaces reside within the isentropic layers used to identify the polar and subtropical jets, are selected to maximize their difference in potential temperature, and serve as reasonable proxies for the polar and subtropical waveguides during the cold season (e.g., Martius et al. 2010; Christenson et al. 2017).

The event classification scheme compares the position of each jet superposition event centroid against the climatological positions of the polar and subtropical waveguides at the start of an event. "Polar dominant" events (Fig. 2a) are those events in which an observation of 2 PVU at the location of the event centroid represents a standardized PV anomaly > 0.5 on the 320-K surface and a standardized PV anomaly > –0.5 on the 350-K surface. Consequently, polar dominant events exhibit a substantial equatorward deviation of the polar jet from its climatological position to superpose with the subtropical jet near its climatological position. "Hybrid" events (Fig. 2b) are those events in which an observation of 2 PVU at the location of the event centroid represents a standardized PV anomaly > 0.5 on the 320-K surface and a standardized PV anomaly < –0.5 on the 350-K surface. Hybrid events, therefore, exhibit a mutual deviation of the polar and subtropical jets from their respective climatological positions to form a superposition. "Subtropical dominant" events (Fig. 2c) are those events in which an observation of 2 PVU at the location of the event centroid represents a standardized PV anomaly < 0.5 on the 320-K surface and a standardized PV anomaly < –0.5 on the 350-K surface. Subtropical dominant events exhibit a substantial poleward deviation of the subtropical jet from its climatological position to superpose with the polar jet near its climatological position. These categories of jet superposition events comprise the spectrum of interactions that can occur between PV anomalies along the polar and subtropical waveguides prior to jet superpositions.

3. Jet superposition event type characteristics

The monthly frequency of North American jet superposition events as a function of event type is shown in Fig. 3. Overall, jet superposition events are most frequent during the months of November and December, and taper off during the remainder of the cold season. This result is consistent with the findings of Christenson et al. (2017; their Fig. 6), whose analysis indicates a greater frequency of North American jet superpositions during November and December compared to January, February, and March. Figure 3 also indicates that subtropical dominant events (N=129) are favored by roughly a 3:2 margin compared to polar dominant events (N=80), suggesting that poleward excursions of the subtropical jet to superpose with the polar jet are more common than the converse evolution. The largest disparity between polar dominant and subtropical dominant events occurs during November and December, when subtropical dominant events are the most frequent event type by a considerable margin. Hybrid events (N=117) are the most frequent event type during January, February, and March.

Figure 4 illustrates the spatial frequency of jet superposition events as a function of event type. Polar dominant events (Fig. 4a) are most frequent along the U.S./Mexico border and along the northern coast of the Gulf of Mexico. The branch of higher spatial frequencies extending towards the northeast U.S. is representative of those polar dominant events that develop at the base of upper-tropospheric troughs and translate downstream within west-southwesterly flow. This direction of jet translation is further apparent when considering the average change in latitude and longitude of a jet superposition event centroid during its life span. Namely, the average polar dominant event develops at subtropical latitudes (e.g., 29.7°N; 102.0°W) and translates towards the east-northeast throughout its life span, consistent with the branch of higher spatial frequencies that extend towards the northeast U.S (Fig. 4a). Hybrid events (Fig. 4b) are most frequent within a 5°-latitude band ranging from 35°N to 40°N, with the largest number of events situated over the southeastern U.S. and western North Atlantic. Hybrid events (34.5°N; 94.3°W) initially develop farther northeast of polar dominant events and translate in a more zonal direction compared to polar dominant events (Table 1).

Subtropical dominant events (Fig. 4c) are characterized by two separate spatial frequency maxima centered on the eastern and western coasts of North America, respectively. Consequently, the average location of jet superposition for subtropical dominant events (46.7°N; 92.1°W) is not representative of the spatial frequency distribution shown in Fig. 4c. This realization motivates partitioning subtropical dominant events into an "eastern" and "western" category based on the position of each individual event centroid relative to the 96°W meridian[3] at the start of an event. A comparison of eastern and western subtropical dominant events shows that eastern events (*N*=76) are more common than western events (*N*=53). Furthermore, eastern (48.5°N; 71.2°W) and western (44.0°N; 122.1°W) subtropical dominant events develop at higher latitudes compared to polar dominant and hybrid events, and both types of subtropical dominant events translate in an east-southeastward direction that is statistically different from polar dominant events (Table 1). The latter result suggests that subtropical dominant events often develop at the apex of upper-tropospheric ridges and subsequently translate downstream within west-northwesterly flow.

4. Jet superposition event type composites

Composite analyses were constructed for each jet superposition event type to examine the synoptic-scale flow evolution during the 48-h period prior to jet superposition. All composites

[3] The forthcoming results are not sensitive to the selection of the 96°W meridian as a differentiator between eastern and western subtropical dominant events.

were calculated by shifting the gridded CFSR and OLR data for each event so that each individual event centroid was collocated with the average starting latitude and longitude for its corresponding event type (Table 1). All CFSR and OLR data were weighted by the cosine of latitude before the data were shifted, and a weighted average of the shifted data was calculated at each grid point within the domain, 10 to 80°N and 150°E to 10°W, to construct the event composites[4]. A two-sided Student's *t*-test was performed on composite 250-hPa geopotential height, precipitable water, and mean sea level pressure anomalies to identify regions that are statistically distinct from climatology at the 99% confidence level. Anomalies of all variables are determined with respect to a 1979–2009 climatology that is calculated every 6 h at each grid point by retaining the first four harmonics of the mean annual cycle. The primary goal of the forthcoming discussion is to determine the dynamical processes that facilitate the development of a steep, single-step tropopause structure during polar, eastern subtropical, and western subtropical dominant events. Hybrid events are not considered further, as the dynamical processes facilitating superposition during those events represent a combination of the processes diagnosed during polar, eastern subtropical, and western subtropical dominant events.

a) Polar dominant events

48 h prior to superposition, a surface cyclone in the Gulf of Alaska is situated within a region of synoptic-scale ascent beneath the poleward-exit region of a zonally extended North Pacific jet (Figs. 5a–c). Anomalous upper-tropospheric ridges are located over the eastern North Pacific and eastern Canada, and an anomalous upper-tropospheric trough is positioned over the southwestern U.S. at this time. A weak surface cyclone is also located within a region of

[4] Although the forthcoming composites are plotted against a geographic map background to provide context for the average evolution of each event type, note that there is variability with respect to the location of each individual jet superposition event.

synoptic-scale ascent downstream of the southwestern U.S. trough and is associated with a zonally oriented band of negative OLR anomalies. These OLR anomalies are suggestive of increased cloud cover along the developing warm front associated with the surface cyclone (not shown).

The eastern North Pacific ridge amplifies during the subsequent 24 h period and exhibits a positive tilt 24 h prior to superposition (Fig. 5d), suggesting a preference for anticyclonic wave breaking (e.g., LC1 events; Thorncroft et al. 1993) to precede polar dominant events. Anticyclonic wave breaking over the eastern North Pacific also contributes to the downstream amplification of the southwestern U.S. trough during the prior 24-h period (Figs. 5a,d). A maximum in 300-hPa geostrophic warm-air advection is diagnosed downstream of the southwestern U.S. trough at this time, suggesting that the along-front ageostrophic circulation induced by strong cyclonic curvature in the base of the southwestern U.S. trough superposes with the across-front ageostrophic circulation induced in the vicinity of the jet to produce ascent beneath the jet axis (Fig. 5e; Keyser and Shapiro 1986, pp. 485–488). In response to the ascent, the surface cyclone intensifies between 48 h and 24 h prior to jet superposition (Figs. 5c,f). Anomalous southerly geostrophic flow that accompanies the surface cyclone contributes to the formation of a corridor of anomalous precipitable water within the warm sector of the cyclone 24 h prior to jet superposition (Fig. 5f). The collocation of precipitable water anomalies, negative OLR anomalies, and synoptic-scale ascent within the warm sector of the surface cyclone suggests that widespread precipitation accompanies the surface cyclone at this time.

The distribution of diabatic heating 24 h prior to polar dominant events is estimated as a residual from the thermodynamic energy equation following Ling and Zhang (2013) as

$$Q = \frac{T}{\theta}\left(\frac{\partial\theta}{\partial t} + u\frac{\partial\theta}{\partial x} + v\frac{\partial\theta}{\partial y} + \omega\frac{\partial\theta}{\partial p}\right), \quad (1)$$

where Q is the diabatic heating term, T is the temperature, θ is the potential temperature, and u, v, and ω are the three-dimensional components of the total wind. The distribution of 500-hPa diabatic heating, as estimated from (1), exhibits considerable overlap with areas of synoptic-scale ascent 24 h prior to superposition (Fig. 6a). This overlap suggests that latent heating acts to erode upper-tropospheric PV downstream of the southwestern U.S. trough and contributes to ridge amplification over eastern North America by the time of superposition (Fig. 5g). Negative PV advection by the three-dimensional divergent circulation[5] along the western flank of the ridge also contributes to the observed ridge amplification over eastern North America (Fig. 6b).

Strong cyclonic curvature in the base of the trough over the southern Plains and 300-hPa geostrophic warm-air advection farther downstream continue to support ascent beneath the jet axis at the time of superposition in the vicinity of the surface cyclone (Figs. 5g–i). As a result, the surface cyclone reaches peak intensity at the time of superposition (Fig. 5i). Precipitable water anomalies, negative OLR anomalies, and synoptic-scale ascent in the vicinity of the surface cyclone also achieve their peak intensity at this time, suggesting that precipitation is maximized in intensity at the time of jet superposition for polar dominant events. All implied areas of precipitation associated with the surface cyclone are located exclusively downstream of the jet superposition event centroid (Figs. 5h,i). Consequently, diabatic heating and the strongest negative PV advection at the level of the dynamic tropopause by the three-dimensional divergent circulation are located too far downstream of the superposed jet to directly facilitate the formation of a single-step tropopause structure during polar dominant events (e.g., Figs. 6a,b). These processes do impact the formation of a jet superposition indirectly, however, by contributing to the aforementioned ridge amplification over eastern North America. Namely,

[5] PV advection by the three-dimensional divergent circulation is defined as the sum of the horizontal PV advection by the irrotational wind and the vertical PV advection.

downstream flow amplification slows the eastward propagation of the upper-tropospheric trough over the southern Plains, prolonging the period during which a jet superposition can develop at the base of the trough.

Upstream of the southern Plains trough, the upper-tropospheric flow pattern is characterized by 300-hPa geostrophic cold-air advection that develops 24 h prior to superposition (Figs. 5d,g). A diagnosis of geostrophic cold-air advection in the presence of strong cyclonic curvature supports descent beneath the jet axis within the jet-entrance region (Fig. 5h; e.g., Keyser and Shapiro 1986, pp. 485–488). As will be shown, the presence of descent beneath the jet-entrance region directly facilitates the formation of a steep, single-step tropopause structure during polar dominant jet events.

Consistent with the diagnosis of geostrophic cold-air advection in the presence of strong cyclonic curvature (Fig. 5g), cross sections perpendicular to the jet axis 12 h prior to superposition (C–C'; Fig. 7a) and at the time of superposition (D–D'; Fig. 7b) depict a region of focused descent beneath and slightly poleward of the jet. This descent accounts for a large fraction of the positive PV advection (90–100%) diagnosed within the tropopause fold at both times and, consequently, for a downward penetration of high-PV air from the lower stratosphere during the 12-h period prior to superposition (Figs. 7a,b). The downward penetration of high-PV air completes the production of a steep, single-step tropopause structure (Fig. 7b).

The cross sections depict the presence of a strong cyclonic PV anomaly on the poleward side of the jet that intensifies in magnitude during the 12-h period prior to superposition, and a weak anticyclonic PV anomaly above 200 hPa on the equatorward side of the jet (Figs. 7a,b). Consequently, the anomalously strong wind speeds that accompany a polar dominant event are driven predominantly by the nondivergent circulation induced by the polar cyclonic PV anomaly.

The lack of a strong anticyclonic PV anomaly on the equatorward side of the jet is not surprising, given that this event type is dominated by the presence of a cyclonically curved jet. The dominance of a polar cyclonic PV anomaly for this event type indicates that knowledge of the creation and subsequent transport of polar cyclonic PV anomalies towards subtropical latitudes is essential towards diagnosing the development of polar dominant jet superpositions.

b) Eastern subtropical dominant events

The large-scale flow pattern 48 h prior to an eastern subtropical dominant event features a zonally oriented upper-tropospheric trough–ridge couplet centered over eastern North America (Fig. 8a). A surface cyclone is positioned within a region of synoptic-scale ascent beneath the jet-entrance region, with a surface anticyclone positioned within a region of weak synoptic-scale descent downstream of the upper-tropospheric ridge (Figs. 8b,c). The longitudinal juxtaposition of the surface cyclone and anticyclone results in anomalous southerly geostrophic flow over eastern North America and the poleward transport of anomalous moisture into the region. The collocation of precipitable water anomalies and negative OLR anomalies within a region of synoptic-scale ascent to the east of the surface cyclone implies that widespread precipitation accompanies the cyclone 48 h prior to jet superposition. Diabatic heating and negative PV advection at the level of the dynamic tropopause by the three-dimensional divergent circulation (not shown) that accompany areas of implied precipitation also contribute to the amplification of the upper-tropospheric ridge on the equatorward side of the double-jet structure during the following 24-h period (Figs. 8a,d).

Geostrophic warm-air advection is diagnosed 24 h prior to superposition at 300 hPa in the entrance region of the developing superposed jet within relatively straight flow (Fig. 8d), implying that the across-front ageostrophic circulation within the jet-entrance region is shifted poleward so as to position ascent beneath the jet axis (Fig. 8e; e.g., Shapiro 1981, 1982; Keyser and Shapiro 1986; Lang and Martin 2012, 2013b). The surface cyclone intensifies in response to this synoptic-scale ascent between 48 h and 24 h prior to jet superposition (Figs. 8c,f). The intensification of the surface cyclone, as well as the downstream surface anticyclone, compared to 48 h prior to superposition results in a strengthened zonal pressure gradient over eastern North America and intensified anomalous southerly geostrophic flow (Fig. 8f). This intensified anomalous southerly geostrophic flow contributes to stronger poleward moisture transport and larger precipitable water anomalies within the warm sector of the surface cyclone 24 h prior to superposition. The distribution of negative OLR anomalies overlaps the positions of the warm and cold fronts associated with the surface cyclone at this time (not shown), and the collocation of these OLR anomalies with both anomalous moisture and synoptic-scale ascent suggests that widespread precipitation persists on the equatorward side of the developing superposed jet.

Diabatic heating and negative PV advection at the level of the dynamic tropopause by the three-dimensional divergent circulation 24 h prior to superposition (Figs. 9a,b) contribute to further amplification of the upper-tropospheric ridge over eastern North America by the time of superposition (Fig. 8g). Consequently, the subtropical waveguide is displaced anomalously poleward of its climatological position (Fig. 8h). Although 300-hPa geostrophic warm-air advection persists along the jet axis at the time of superposition, areas of warm-air advection are now focused in the jet-exit region rather than in the jet-entrance region, as they were 24 h earlier (Figs. 8d,g). The presence of geostrophic warm-air advection within the jet-exit region implies that the across-front ageostrophic circulation in that location is shifted equatorward so as to position ascent beneath the jet axis (Figs. 8g,h; Shapiro 1981, 1982; Keyser and Shapiro 1986; Lang and Martin 2012, 2013b). Although the surface cyclone remains aligned with this area of ascent, the surface cyclone does not intensify during the 24-h period prior to superposition (Figs. 8f,i). Additionally, precipitable water anomalies and negative OLR anomalies decrease in magnitude during the prior 24-h period. Together, these observations imply that surface cyclogenesis and widespread precipitation tend to lead the development of eastern subtropical dominant events, rather than peak at the time of superposition as observed during polar dominant events.

Farther upstream of the surface cyclone, 300-hPa geostrophic cold-air advection is diagnosed within the jet-entrance region at the time of jet superposition (Fig. 8g). The presence of geostrophic cold-air advection within the jet-entrance region suggests that the across-front ageostrophic circulation in that location is shifted equatorward so as to position descent beneath the jet axis (Fig. 8h). Referred to as the "Shapiro effect" by Rotunno et al. (1994), this process is strongly conducive to upper-tropospheric frontogenesis and the concomitant development of a tropopause fold (e.g., Shapiro 1981, 1982; Keyser and Pecnick 1985; Keyser and Shapiro 1986; Rotunno et al. 1994; Schultz and Doswell 1999; Schultz and Sanders 2002; Lang and Martin 2010, 2012, 2013a; Schultz 2013; Martin 2014; Winters and Martin 2016, 2017). To investigate the formation of the single-step tropopause structure further, we analyze fields along a vertical cross section (E–E') immediately upstream of the jet superposition centroid and perpendicular to the jet axis 12 h prior to superposition (Fig. 10a) and at the time of superposition (Fig. 10b).

Figure 10a depicts an area of ascent directly beneath the jet 12 h prior to superposition, consistent with the presence of geostrophic warm-air advection along the jet axis and ascent in the vicinity of the surface cyclone during the 24-h period prior to superposition (Figs. 8d–i). This ascent is responsible for a large fraction (~80–95%) of the negative PV advection diagnosed along the tropopause within the cross section, and acts to locally steepen the tropopause during the 12-h period prior to superposition (Figs. 10a,b). Given that this ascent coincides with a broad region of diabatic heating (Fig. 9a), latent heating also contributes to an erosion of upper-tropospheric PV on the equatorward side of the jet during the 12-h period prior to superposition (Figs. 10a,b). In combination, the negative PV advection diagnosed along the tropopause and the latent heating associated with moist ascent underscore the important contribution from moist ascent during the formation of eastern subtropical dominant events. A narrow zone of descent develops beneath the jet at the time of superposition (Fig. 10b), in agreement with the diagnosis of geostrophic cold-air advection within the jet-entrance region at this time (Fig. 8g). This descent is associated with positive PV advection in the base of the tropopause fold (Fig. 10b), and facilitates a downward transport of high-PV air that contributes to the resultant single-step tropopause structure associated with the jet superposition.

In contrast to polar dominant events (Figs. 7a,b), the superposed jet in eastern subtropical dominant events (Figs. 10a,b) is characterized by the horizontal juxtaposition of a polar cyclonic and a tropical anticyclonic PV anomaly during the 12-h period prior to superposition. This configuration of upper-tropospheric PV anomalies strongly resembles the conceptual model shown within Fig. 1c and suggests that the nondivergent circulations induced by each PV anomaly superpose to produce the anomalously strong wind speeds associated with eastern subtropical dominant events. Consequently, knowledge of the creation, transport towards middle latitudes, and phasing of polar cyclonic and tropical anticyclonic PV anomalies is critical towards correctly diagnosing the development of this jet superposition event type.

c) Western subtropical dominant events

The development of western subtropical dominant events features the meridional juxtaposition of an anomalous upper-tropospheric trough at polar latitudes and an anomalous ridge at subtropical latitudes near the west coast of North America 48 h prior to superposition, which results in a zonally extended North Pacific jet (Fig. 11a). A surface cyclone is situated beneath the poleward-exit region of the jet, and is characterized by an elongated corridor of anomalous precipitable water on the equatorward flank of the cyclone (Fig. 11c). The aspect ratio of this corridor of anomalous precipitable water strongly resembles the character of landfalling western U.S. atmospheric rivers (e.g., Newell et al. 1992; Zhu and Newell, 1998; Ralph et al. 2004, 2018, 2019; Cannon et al. 2018), and is collocated with broad regions of 300-hPa geostrophic warm-air advection (Fig. 11a) and negative OLR anomalies along the jet axis (Fig. 11c). Similar to eastern subtropical dominant events, the presence of geostrophic warm-air advection in relatively straight flow favors ascent and implied precipitation beneath the jet axis in the vicinity of the Pacific Northwest at this time (Fig. 11b). Orographic ascent likely also contributes to the production of precipitation during these events, given that anomalous geostrophic winds near the surface are oriented perpendicular to the west coast of North America.

The distribution of diabatic heating and negative PV advection at the level of the dynamic tropopause by the three-dimensional divergent circulation (not shown) that accompany the aforementioned ascent contribute to the amplification of the eastern North Pacific ridge between 48 h and 24 h prior to superposition (Figs. 11a,d). The anomalous upper-tropospheric trough poleward of the developing superposed jet also amplifies compared to the prior time, which results in a strengthened meridional geopotential height gradient and an increase in upper-tropospheric wind speeds. The surface cyclone intensifies compared to the prior time beneath the poleward-exit region of the developing superposed jet, and is characterized by a stronger and more spatially coherent corridor of anomalous precipitable water on its equatorward flank (Figs.

11c,f). The overlap of anomalous precipitable water with negative OLR anomalies, 300-hPa geostrophic warm-air advection, and onshore lower-tropospheric geostrophic flow (Figs. 11d,f) suggests that widespread precipitation persists along the west coast of North America 24 h prior to superposition in conjunction with ascent beneath the jet axis (Fig. 11e).

The anomalous upper-tropospheric ridge near the west coast of North America achieves peak intensity at the time of jet superposition in response to diabatic heating and negative PV advection by the three-dimensional divergent circulation diagnosed in the vicinity of the jet 24 h prior to superposition (Figs. 12a,b). The upper-tropospheric trough also reaches peak intensity at the time of superposition resulting in an increase in wind speed along the axis of the superposed jet compared to 24 h prior to superposition (Figs. 11d,g). The surface cyclone remains located within a region of ascent beneath the poleward-exit region of the superposed jet (Figs. 11e,h), with its associated corridor of anomalous precipitable water focused farther south than at prior times along the central California coast (Figs. 11c,f,i). Notably, both negative OLR anomalies and sea level pressure anomalies decrease in magnitude during the 24-h period prior to superposition (Figs. 11f,i). Similar to eastern subtropical dominant events, this observation suggests that surface cyclogenesis and widespread precipitation lead the formation of western subtropical dominant events.

As in eastern subtropical dominant events, 300-hPa geostrophic cold-air advection is diagnosed within the jet-entrance region at the time of superposition (Fig. 11g), suggesting that the across-front ageostrophic circulation within the jet-entrance region is shifted equatorward so as to position descent beneath the jet axis (Fig. 11h). To examine the impact of this descent, as well as moist ascent, on the production of a single-step tropopause structure during the 12-h period prior to superposition, a cross section (F–F’) is constructed immediately upstream of the jet superposition centroid and perpendicular to the jet axis. Figure 13a depicts a focused region of ascent beneath the developing superposed jet 12 h prior to superposition, consistent with the presence of geostrophic warm-air advection along the jet axis prior to superposition (Fig. 11d). This ascent accounts for a large fraction of the negative PV advection diagnosed along the tropopause within the cross section (~120%), and acts to locally steepen the tropopause. Given that this ascent is collocated with a maximum in diabatic heating (Fig. 12a), the erosion of upper-tropospheric PV that accompanies latent heating acts to further steepen the tropopause on the equatorward side of the jet during the 12-h period prior to superposition (Figs. 13a,b).

A narrow zone of descent is diagnosed beneath the jet at the time of superposition (Fig. 13b). As in eastern subtropical dominant events, this descent accounts for positive PV advection within the tropopause fold and a downward penetration of high-PV air from the lower stratosphere. The downward transport of high-PV air from the lower stratosphere further steepens the tropopause and contributes to the formation of the single-step tropopause structure that results at the time of superposition. Both cross sections shown in Figs. 13a,b also demonstrate that the superposed jet is characterized by the horizontal juxtaposition of a polar cyclonic and tropical anticyclonic PV anomaly near the tropopause. Consequently, the increase in wind speed in the vicinity of western subtropical dominant events results from the superposition of the nondivergent circulations induced by each PV anomaly. Therefore, as in eastern subtropical dominant events, knowledge of the creation, transport towards middle latitudes, and phasing of polar cyclonic and tropical anticyclonic PV anomalies is critical for correctly diagnosing the production of a western subtropical dominant event.

5. Summary

This study classifies North American jet superposition events into characteristic event types based on the relative deviations of the polar and subtropical jets from their respective climatological latitude bands, and investigates the dynamical mechanisms that facilitate the production of a steep, single-step tropopause structure during polar, eastern subtropical, and western subtropical dominant jet superposition events. The dynamical evolutions associated with each jet superposition event type are summarized via the conceptual models presented in Fig. 14.

Polar dominant events (Fig. 14a) are often preceded by anticyclonic wave breaking over the eastern North Pacific during the 48-h period prior to jet superposition. Anticyclonic wave breaking subsequently facilitates the equatorward transport of a polar cyclonic PV anomaly towards subtropical latitudes, allowing the polar jet to superpose with the subtropical jet near the climatological position of the subtropical jet. A surface cyclone develops beneath the poleward-exit region of the developing superposed jet and is maximized in intensity at the time of jet superposition. The surface cyclone features anomalous poleward moisture transport within its warm sector, and is associated with implied precipitation that also is maximized in intensity at the time of superposition. The surface cyclone and areas of implied precipitation are located exclusively downstream of the jet superposition. Therefore, moist ascent does not directly impact the formation of a single-step tropopause structure during polar dominant events. Instead, strong cyclonic curvature and upper-tropospheric geostrophic cold-air advection support descent beneath the entrance region of the developing superposed jet. This descent directly facilitates the development of a single-step tropopause structure during polar dominant events.

A surface cyclone and implied precipitation develop beneath the equatorward-entrance region of developing eastern subtropical dominant jet superpositions, and tend to be maximized in intensity prior to jet superposition (Fig. 14b). Moist ascent, therefore, directly influences the development of a single-step tropopause structure during eastern subtropical dominant events by locally steepening the tropopause via negative PV advection by the three-dimensional divergent circulation and via the diabatic erosion of upper-tropospheric PV on the equatorward side of the jet. Upper-tropospheric geostrophic cold-air advection develops within the jet-entrance region during the 24-h period preceding jet superposition, implying an equatorward shift of the across-front ageostrophic circulation in that location so as to position descent beneath the jet axis. This descent acts to steepen the tropopause further by the time of superposition via the downward transport of high-PV air from the lower stratosphere, thereby completing the formation of a single-step tropopause structure.

Western subtropical dominant events (Fig. 14c) are characterized by a surface cyclone that develops beneath the poleward-exit region of the jet, rather than beneath the equatorward-entrance region of the jet as observed during eastern subtropical dominant events (Fig. 14b). The surface cyclone is accompanied by a zonally oriented corridor of anomalous moisture that strongly resembles the character of a western U.S. atmospheric river. Widespread ascent and precipitation diagnosed along this corridor of anomalous moisture are maximized in intensity prior to the development of a jet superposition, as in eastern subtropical events, and directly influence the production of a single-step tropopause structure by steepening the tropopause via negative PV advection by the three-dimensional divergent circulation and via the diabatic erosion of upper-tropospheric PV on the equatorward side of the jet. Upper-tropospheric geostrophic cold-air advection develops within the jet-entrance region by the time of superposition, indicating descent beneath the jet axis in that location. Consequently, descent facilitates the production of western subtropical dominant jet superpositions by contributing to the formation of a single-step tropopause structure.

The event types considered in this study reveal the varied roles that moist processes play during the production of North American jet superpositions. Namely, moist ascent appears to directly contribute to the formation of a single-step tropopause structure during eastern and western subtropical dominant events, whereas moist ascent is located too far downstream of polar dominant events to directly impact the production of a single-step tropopause structure during those events. This difference motivates future work investigating the relative importance of moist ascent during jet superposition events. Of particular interest is whether the omission of diabatic heating during the 48-h period prior to each jet superposition event type would result in the formation of a jet superposition. It is hypothesized that both types of subtropical dominant events would be more sensitive to the omission of diabatic heating than polar dominant events, given the influence of diabatic heating in restructuring the tropopause during both subtropical dominant event types.

A key result from this study is that descent beneath the entrance region of a developing superposed jet occurs for each event type. This result motivates two questions concerning the production of descent during jet superposition events. First, following the analyses conducted by Keyser et al. (1992), Martin (2006a), and Martin (2014), what fraction of the observed descent is due to across-front ageostrophic circulations that arise due to frontogenetical processes within the confluent jet-entrance region (i.e., divergence of the across-front component of the **Q**-vector) versus along-front couplets of vertical motion that arise due to flow curvature and are of the scale of baroclinic waves (i.e., divergence of the along-front component of the **Q**-vector)? The respective large-scale evolutions discussed in section 4 demonstrate that both of these processes appear to operate to varying degrees within each event type. Second, what fraction of the observed descent within each event type can be attributed to the three-dimensional circulations that accompany upper-tropospheric PV anomalies along the polar and subtropical waveguides? The answer to the second question, in particular, is likely to reveal the relative influence that polar cyclonic and tropical anticyclonic PV anomalies have on the production of a single-step tropopause structure during each jet superposition event type.

North American jet superposition events during the cool season are most frequent during November and December, rather than during January and February as they are in the western North Pacific and northern Africa (Christenson et al. 2017; their Fig. 6). Given that North American jet superpositions are generally preceded by the development of an amplified upper-tropospheric flow pattern, the lower frequency of North American jet superposition events during January and February may be tied to the lower frequency of Rossby wave breaking events in the eastern North Pacific during the winter compared to the fall and spring (e.g., Nakamura 1992; Abatzoglou and Magnusdottir 2006; Bowley et al. 2019). Additionally, prior case study work suggests that jet superpositions can form outside of the cold season (i.e., Christenson 2013; Winters and Martin 2014, 2016). Therefore, subsequent examinations of jet superposition events should modify the jet identification scheme employed within this study to identify North American jet superposition events that occur during the fall and spring. A comparison between jet superposition events across seasons has the potential to determine the degree to which the dynamical processes and the types of sensible weather impacts that accompany jet superposition events vary as a function of season.

The composite large-scale flow patterns associated with jet superposition events bear a resemblance to large-scale flow patterns associated with continental U.S. extreme precipitation events during the cool season (Moore et al. 2015, 2019). A cursory examination of individual events within each jet superposition event type indicates, however, that a jet superposition is not necessarily a sufficient condition for the development of high-impact weather. Future work that differentiates between jet superposition environments that lead to high-impact weather events versus those that result in null events, and whether those relationships depend on the magnitude and/or life span of a jet superposition event, offers the potential to benefit operational forecasts of high-impact weather.

Last, future work that examines the relationship between jet superpositions and large-scale teleconnection patterns, such as the Pacific–North American pattern (e.g., Wallace and Gutzler 1981) and the Madden–Julian Oscillation (e.g., Madden and Julian 1972), may reveal large-scale flow regimes that present an increased likelihood for North American jet superpositions. The development and subsequent downstream translation of superposed jets can also effectively reconfigure the large-scale flow pattern over the North Atlantic. Therefore, knowledge of the impact that North American jet superpositions can have on the downstream large-scale flow pattern may have important implications for operational forecasts for western Europe.

Data Availability Statement

All datasets used in this study are publicly available for download from the NOAA Earth Science Research Laboratory Physical Sciences Division or from the Research Data Archive at NCAR. A list of all jet superposition events and all computer programs written to perform the data analysis are available from the first author upon request.

Acknowledgments

This work was supported by the National Science Foundation through an AGS Postdoctoral Research Fellowship (AGS-1624316) held at the University at Albany, State University of New York by ACW. We thank the editor, David M. Schultz, and three anonymous reviewers for their constructive comments on a prior version of this manuscript.

References

Abatzoglou, J. T., and G. Magnusdottir, 2006: Planetary wave breaking and nonlinear reflection: Seasonal cycle and interannual variability. *J. Climate*, **19**, 6139–6152, doi: 10.1175/JCLI3968.1.

Agustí-Panareda, A., C. D. Thorncroft, G. C. Craig, and S. L. Gray, 2004: The extratropical transition of Hurricane Irene (1999): A potential-vorticity perspective. *Quart. J. Roy. Meteor. Soc.*, **130**, 1047–1074, doi: 10.1256/qj.02.140.

Ahmadi-Givi, F., G. C. Craig, and R. S. Plant, 2004: The dynamics of a midlatitude cyclone with very strong latent-heat release. *Quart. J. Roy. Meteor. Soc.*, **130**, 295–323, doi: 10.1256/qj.02.226.

Archambault, H. M., L. F. Bosart, D. Keyser, and J. M. Cordeira, 2013: A climatological analysis of the extratropical flow response to recurving western North Pacific tropical cyclones. *Mon. Wea. Rev.*, **141**, 2325–2346, doi: 10.1175/MWR-D-12-00257.1.

Archambault, H. M., D. Keyser, L. F. Bosart, C. A. Davis, and J. M. Cordeira, 2015: A composite perspective of the extratropical flow response to recurving western North Pacific tropical cyclones. *Mon. Wea. Rev.*, **143**, 1122–1141, doi: 10.1175/MWR-D-14-00270.1.

Bowley, K. A., J. R. Gyakum, and E. H. Atallah, 2019: A new perspective toward cataloging Northern Hemisphere Rossby wave breaking on the dynamic tropopause. *Mon. Wea. Rev.*, **147**, 409–431, doi: 10.1175/MWR-D-18-0131.1.

Cannon, F., C. W. Hecht, J. M. Cordeira, and F. M. Ralph, 2018: Synoptic and mesoscale forcing of southern California extreme precipitation. *J. Geophys. Res.: Atmospheres*, **123**, 13714–13730, doi: 10.1029/2018JD029045.

Cavallo, S. M., and G. J. Hakim, 2009: Potential vorticity diagnosis of a tropopause polar cyclone. *Mon. Wea. Rev.*, **137**, 1358–1371, doi: 10.1175/2008MWR2670.1.

Cavallo, S. M., and G. J. Hakim, 2010: Composite structure of tropopause polar cyclones. *Mon. Wea. Rev.*, **138**, 3840–3857, doi: 10.1175/2010MWR3371.1.

Cavallo, S. M., and G. J. Hakim, 2012: Radiative impact on tropopause polar vortices over the Arctic. *Mon. Wea. Rev.*, **140**, 1683–1702, doi: 10.1175/MWR-D-11-00182.1.

Cavallo, S. M., and G. J. Hakim, 2013: Physical mechanisms of tropopause polar vortex intensity change. *J. Atmos. Sci.*, **70**, 3359–3373, doi: 10.1175/JAS-D-13-088.1.

Christenson, C. E., 2013: A synoptic-climatology of Northern Hemisphere polar and subtropical jet superposition events. M.S. thesis, University of Wisconsin–Madison, 62 pp.

Christenson, C. E., J. E. Martin, Z. J. Handlos, 2017: A synoptic climatology of Northern Hemisphere, cold season polar and subtropical jet superposition events. *J. Climate*, **30**, 7231–7246, doi: 10.1175/JCLI-D-16-0565.1.

Fröhlich, L., P. Knippertz, A. H. Fink, and E. Hohberger, 2013: An objective climatology of tropical plumes. *J. Climate*, **26**, 5044–5060, doi: 10.1175/JCLI-D-12-00351.1.

Grams, C. M., H. Wernli, M. Böttcher, J. Čampa, U. Corsmeier, S. C. Jones, J. H. Keller, C.-J. Lenz, and L. Wiegand, 2011: The key role of diabatic processes in modifying the upper-tropospheric wave guide: A North Atlantic case-study. *Quart. J. Roy. Meteor. Soc.*, **137,** 2174–2193, doi: 10.1002/qj.891.

Grams, C. M., S. C. Jones, C. A. Davis, P. A. Harr, and M. Weissmann, 2013: The impact of Typhoon Jangmi (2008) on the midlatitude flow. Part I: Upper-level ridgebuilding and modification of the jet. *Quart. J. Roy. Meteor. Soc.,* **139,** 2148−2164, doi: 10.1002/qj.2091.

Grams, C. M., and H. M. Archambault, 2016: The key role of diabatic outflow in amplifying the midlatitude flow: A representative case study of weather systems surrounding western North Pacific extratropical transition. *Mon. Wea. Rev.*, **144**, 3847–3869, doi: 10.1175/MWR-D-15-0419.1.

Hakim, G. J., 2000: Climatology of coherent structures on the extratropical tropopause. *Mon. Wea. Rev.*, **128**, 385–406, doi: 10.1175/1520-0493%282000%29128<0385%3ACOCSOT>2.0.CO%3B2.

Hakim, G. J., L. F. Bosart, and D. Keyser, 1995: The Ohio Valley wave-merger cyclogenesis event of 25–26 January 1978. Part I: Multiscale case study. *Mon. Wea. Rev.*, **123**, 2663–2692, doi: 10.1175/1520-0493(1995)123<2663:TOVWMC>2.0.CO;2.

Hakim, G. J., D. Keyser, and L. F. Bosart, 1996: The Ohio Valley wave-merger cyclogenesis event of 25–26 January 1978. Part II: Diagnosis using quasigeostrophic potential vorticity inversion. *Mon. Wea. Rev.*, **124**, 2176–2205, doi: 10.1175/1520-0493(1996)124<2176:TOVWMC>2.0.CO;2.

Handlos, Z. J., and J. E. Martin, 2016: Composite analysis of large-scale environments conducive to west Pacific polar/subtropical jet superposition. *J. Climate*, **29**, 7145–7165, doi: 10.1175/JCLI-D-16-0044.1.

Iskenderian, H., 1995: A 10-year climatology of Northern Hemisphere tropical cloud plumes and their composite flow patterns. *J. Climate*, **8**, 1630–1637, doi: 10.1175/1520-0442(1995)008<1630:AYCONH>2.0.CO;2.

Kalnay, E., and Coauthors, 1996: The NCEP/NCAR 40-Year Reanalysis Project. *Bull. Amer. Meteor. Soc.*, **77**, 437–470, doi: 10.1175/1520-0477(1996)077,0437:TNYRP.2.0.CO;2.

Keyser, D., and M. J. Pecnick, 1985: A two-dimensional primitive equation model of frontogenesis forced by confluence and horizontal shear. *J. Atmos. Sci.*, **42**, 1259–1282, doi: 10.1175/1520-0469(1985)042,1259:ATDPEM.2.0.CO;2.

Keyser, D., and M. A. Shapiro, 1986: A review of the structure and dynamics of upper-level frontal zones. *Mon. Wea. Rev.*, **114**, 452–499, doi: 10.1175/1520-0493(1986)114<0452:AROTSA>2.0.CO;2.

Keyser, D., B. D. Schmidt, and D. G. Duffy, 1992: Quasigeostrophic vertical motions diagnosed from along- and cross-isentrope components of the Q vector. *Mon. Wea. Rev.*, **120**, 731–741, doi: 10.1175/1520-0493%281992%29120<0731%3AQVMDFA>2.0.CO%3B2.

Kistler, R., and Coauthors, 2001: The NCEP–NCAR 50-Year Reanalysis: Monthly means CD-ROM and documentation. *Bull. Amer. Meteor. Soc.*, **82**, 247–267, doi: 10.1175/ 1520-0477(2001)082,0247:TNNYRM.2.3.CO;2.

Koteswaram, P., 1953: An analysis of the high tropospheric wind circulation over India in winter. *Indian J. Meteor. Geophys.*, **4**, 13–21.

Koteswaram, P., and S. Parthasarathy, 1954: The mean jet stream over Indian in the pre-monsoon and post-monsoon seasons and vertical motions associated with subtropical jet streams. *Indian J. Meteor. Geophys.*, **5**, 138–156.

Krishnamurti, T. N., 1961: The subtropical jet stream of winter. *J. Meteor.*, **18**, 172–191, doi: 10.1175/1520-0469(1961)018<0172:TSJSOW>2.0.CO;2.

Lang, A. A., and J. E. Martin, 2010: The influence of rotational frontogenesis and its associated shearwise vertical motion on the development of an upper-level front. *Quart. J. Roy. Meteor. Soc.*, **136**, 239–252, doi: 10.1002/qj.551.

Lang, A. A., and J. E. Martin, 2012: The structure and evolution of lower stratospheric frontal zones. Part I: Examples in northwesterly and southwesterly flow. *Quart. J. Roy. Meteor. Soc.*, **138**, 1350–1365, doi: 10.1002/qj.843.

Lang, A. A., and J. E. Martin, 2013a: Reply to comments on 'The influence of rotational frontogenesis and its associated shearwise vertical motion on the development of an upper-level front.' *Quart. J. Roy. Meteor. Soc.*, **139**, 273–279, doi: 10.1002/qj.2042.

Lang, A. A., and J. E. Martin, 2013b: The structure and evolution of lower stratospheric frontal zones: Part II: The influence of tropospheric ascent on lower stratospheric frontal development. *Quart. J. Roy. Meteor. Soc.*, **139**, 1798–1809, doi: 10.1002/qj.2074.

Lee, S., and H.-K. Kim, 2003: The dynamical relationship between subtropical and eddy-driven jets. *J. Atmos. Sci.*, **60**, 1490–1503, doi: 10.1175/1520-0469%282003%29060<1490%3ATDRBSA>2.0.CO%3B2.

Liebmann, B., and C. A. Smith, 1996: Description of a complete (interpolated) outgoing longwave radiation dataset. *Bull. Amer. Meteor. Soc.*, **77**, 1275–1277.

Ling, J. and C. Zhang, 2013: Diabatic heating profiles in recent global reanalyses. *J. Climate*, **26**, 3307–3325, doi: 10.1175/JCLI-D-12-00384.1.

Loewe, F., and V. Radok, 1950: A meridional aerological cross section in the southwest Pacific. *J. Meteor.*, **7**, 58–65, doi: 10.1175/1520-0469(1950)007<0058:AMACSI>2.0.CO;2.

Madden, R. A., and P. R. Julian, 1972: Description of global-scale circulation cells in the tropics with a 40–50 day period. *J. Atmos. Sci.*, **29**, 1109–1123, doi: 10.1175/1520-0469(1972)0292.0.CO;2.

Martin J. E., 2006a. The role of shearwise and transverse quasigeostrophic vertical motions in the midlatitude cyclone life cycle. *Mon. Wea. Rev.*, **134**, 1174–1193, doi: 10.1175/MWR3114.1.

Martin, J. E., 2006b: *Mid-Latitude Atmospheric Dynamics. A First Course*. John Wiley and Sons, Ltd., 324 pp.

Martin, J. E., 2014: Quasi-geostrophic diagnosis of the influence of vorticity advection on the development of upper level jet-front systems. *Quart. J. Roy. Meteor. Soc.*, **140**, 2658–2671, doi: 10.1002/qj.2333.

Martius, O., C. Schwierz, and H. C. Davies, 2010: Tropopause-level waveguides. *J. Atmos. Sci.*, **67**, 866–879, doi: 10.1175/2009JAS2995.1.

McTaggart-Cowan, R., L. F. Bosart, J. R. Gyakum, and E. H. Atallah, 2007: Hurricane Katrina (2005). Part II: Evolution and hemispheric impacts of a diabatically generated warm pool. *Mon. Wea. Rev.*, **135**, 3927–3949, doi: 10.1175/2007MWR2096.1.

Mohri, K., 1953: On the fields of wind and temperature over Japan and adjacent waters during winter of 1950–1951. *Tellus*, **5**, 340–358, doi: 10.3402/tellusa.v5i3.8582.

Moore, B. J., P. J. Neiman, F. M. Ralph, and F. E. Barthold, 2012: Physical processes associated with heavy flooding rainfall in Nashville, Tennessee, and vicinity during 1–2 May 2010: The role of an atmospheric river and mesoscale convective systems. *Mon. Wea. Rev.*, **140**, 358–378, doi: 10.1175/MWR-D-11-00126.1.

Moore, B. J., K. M. Mahoney, E. M. Sukovich, R. Cifelli, and T. M. Hamill, 2015: Climatology and environmental characteristics of extreme precipitation events in the southeastern United States. *Mon. Wea. Rev.*, **143**, 718–741, doi: 10.1175/MWR-D-14-00065.1.

Moore, B. J., D. Keyser, and L. F. Bosart, 2019: Linkages between extreme precipitation events in the central and eastern United States and Rossby wave breaking. *Mon. Wea. Rev.*, **147**, 3327–3349, doi: 10.1175/MWR-D-19-0047.1.

Nakamura, H., 1992: Midwinter suppression of baroclinic wave activity in the Pacific. *J. Atmos. Sci.*, **49**, 1629–1642, doi: 10.1175/1520-0469%281992%29049<1629%3AMSOBWA>2.0.CO%3B2.

Namias, J., and P. F. Clapp, 1949: Confluence theory of the high tropospheric jet stream. *J. Meteor.*, **6**, 330–336, doi: 10.1175/1520-0469(1949)006<0330:CTOTHT>2.0.CO;2.

Newell, R. E., N. E. Newell, Y. Zhu, and C. Scott, 1992: Tropospheric rivers?—A pilot study. *Geophys. Res. Lett.*, **19**, 2401–2404, doi: 10.1029/92GL02916.

Newton, C. W., 1954: Frontogenesis and frontolysis as a three-dimensional process. *J. Meteor.*, **11**, 449–461, doi: 10.1175/1520-0469(1954)011<0449:FAFAAT>2.0.CO;2.

Palmén, E., and C. W. Newton, 1948: A study of the mean wind and temperature distribution in the vicinity of the polar front in winter. *J. Meteor.*, **5**, 220–226, doi: 10.1175/1520-0469(1948)005<0220:ASOTMW>2.0.CO;2.

Palmén, E., and C. W. Newton, 1969: *Atmospheric Circulation Systems: Their Structure and Physical Interpretation*. Academic Press, 603 pp.

Pyle, M. E., D. Keyser, and L. F. Bosart, 2004: A diagnostic study of jet streaks: Kinematic signatures and relationship to coherent tropopause disturbances. *Mon. Wea. Rev.*, **132**, 297–319, doi: 10.1175/1520-0493(2004)132<0297:ADSOJS>2.0.CO;2.

Ralph, F. M., P. J. Neiman, and G. A. Wick, 2004: Satellite and CALJET aircraft observations of atmospheric rivers over the eastern North Pacific Ocean during the winter of

1997/98. *Mon. Wea. Rev.*, **132**, 1721–1745, doi: 10.1175/1520-0493(2004)132<1721:SACAOO>2.0.CO;2.

Ralph, F. M., M. D. Dettinger, M. M. Cairns, T. J. Galarneau, and J. Eylander, 2018: Defining "atmospheric river": How the *Glossary of Meteorology* helped resolve a debate. *Bull. Amer. Meteor. Soc.*, **99**, 837–839, doi: 10.1175/BAMS-D-17-0157.1

Ralph, F. M., and Coauthors, 2019: A scale to characterize the strength of impacts of atmospheric rivers. *Bull. Amer. Meteor. Soc.*, **100**, 269–289, doi: 10.1175/BAMS-D-18-0023.1.

Riehl, H., 1962: Jet streams of the atmosphere. Dept. of Atmospheric Science Tech. Rep. 32, Colorado State University, Fort Collins, CO, 117 pp.

Rotunno, R., W. C. Skamarock, and C. Snyder, 1994: An analysis of frontogenesis in numerical simulations of baroclinic waves. *J. Atmos. Sci.*, **51**, 3373–3398, doi: 10.1175/1520-0469(1994)051,3373:AAOFIN.2.0.CO;2.

Roundy, P. E., K. MacRitchie, J. Asuma, and T. Melino, 2010: Modulation of the global atmospheric circulation by combined activity in the Madden–Julian oscillation and the El Niño–Southern Oscillation during boreal winter. *J. Climate*, **23**, 4045–4059, doi: 10.1175/2010JCLI3446.1.

Saha, S., and Coauthors, 2010: The NCEP Climate Forecast System Reanalysis. *Bull. Amer. Meteor. Soc.*, **91**, 1015–1057, doi: 10.1175/2010BAMS3001.1.

Schultz, D. M., 2013: Comment on 'The influence of rotational frontogenesis and its associated shearwise vertical motion on the development of an upper-level front' by A. A. Lang and J. E. Martin (January 2010, 136: 239–252). *Quart. J. Roy. Meteor. Soc.*, **139**, 269–272, https://doi.org/10.1002/qj.1871.

Schultz, D. M., and C. A. Doswell III, 1999: Conceptual models of upper-level frontogenesis in south-westerly and north-westerly flow. *Quart. J. Roy. Meteor. Soc.*, **125**, 2535–2562, doi: 10.1002/qj.49712555910.

Schultz, D. M., and F. Sanders, 2002: Upper-level frontogenesis associated with the birth of mobile troughs in northwesterly flow. *Mon. Wea. Rev.*, **130**, 2593–2610, doi: 10.1175/1520-0493 (2002)130,2593:ULFAWT.2.0.CO;2.

Shapiro, M. A., 1981: Frontogenesis and geostrophically forced secondary circulations in the vicinity of jet stream-frontal zone systems. *J. Atmos. Sci.*, **38**, 954–973, doi: 10.1175/1520-0469(1981)038<0954:FAGFSC>2.0.CO;2.

Shapiro, M. A., 1982: *Mesoscale weather systems of the central United States.* CIRES, 78 pp.

Shapiro, M. A., and D. Keyser, 1990: Fronts, jet streams, and the tropopause. *Extratropical Cyclones: The Erik Palmén Memorial Volume*, C. Newton and E. O. Holopainen, Eds., Amer. Meteor. Soc., 167–191.

Son, S.-W., and S. Lee, 2005: The response of westerly jets to thermal driving in a primitive equation model. *J. Atmos. Sci.*, **62**, 3741–3757, doi: 10.1175/JAS3571.1.

Starr, V. P., 1948: An essay on the general circulation of the earth’s atmosphere. *J. Meteor.*, **5**, 39–43.

Sutcliffe, R. C., and J. K. Bannon, 1954: Seasonal changes in the upper-air conditions in the Mediterranean Middle East area. *Proc. Int. Association of Meteorology*, Rome, Italy, Int. Union of Geodesy and Geophysics. 322–334.

Thorncroft, C. D., B. J. Hoskins, and M. E. McIntyre, 1993: Two paradigms of baroclinic-wave life-cycle behaviour. *Quart. J. Roy. Meteor. Soc.*, **119**, 17–55, doi: 10.1002/qj.49711950903.

Wallace, J. M., and D. S. Gutzler, 1981: Teleconnections in the geopotential height field during the Northern Hemisphere winter. *Mon. Wea. Rev.*, **109**, 784–812, doi: 10.1175/1520- 809 0493(1981)1092.0.CO;2.

Winters, A. C., and J. E. Martin, 2014: The role of a polar/subtropical jet superposition in the May 2010 Nashville flood. *Wea. Forecasting*, **29**, 954–974, doi: 10.1175/WAF-D-13-00124.1.

Winters, A. C., and J. E. Martin, 2016: Synoptic and mesoscale processes supporting vertical superposition of the polar and subtropical jets in two contrasting cases. *Quart. J. Roy. Meteor. Soc.*, **142**, 1133–1149, doi: 10.1002/qj.2718.

Winters, A. C., and J. E. Martin, 2017: Diagnosis of a North American polar–subtropical jet superposition employing piecewise potential vorticity inversion. *Mon. Wea. Rev.*, **145**, 1853–1873, doi: 10.1175/MWR-D-16-0262.1.

Yeh, T. C., 1950: The circulation of the high troposphere over China in the winter of 1945–46. *Tellus*, **2**, 173–183, doi: 10.3402/tellusa.v2i3.8548.

Zhu, Y., and R. E. Newell, 1998: A proposed algorithm for moisture fluxes from atmospheric rivers. *Mon. Wea. Rev.*, **126**, 725–735, doi: 10.1175/1520-0493(1998)126<0725:APAFMF>2.0.CO;2.

Tables

Jet Superposition Characteristics				
	Avg. Starting Latitude	Avg. Starting Longitude	Avg. ΔLatitude	Avg. ΔLongitude
Polar Dominant (N= 80)	29.7°N	102.0°W	+3.4°$^{\mathrm{sew}}$	+12.3°
Hybrid (N=117)	34.5°N	94.3°W	+0.9°	+11.2°
Subtropical Dominant (N=129)	46.7°N	92.1°W	–1.0°$^{\mathrm{p}}$	+12.3°
East Subtropical Dominant (N=76)	48.5°N	71.2°W	–1.1°$^{\mathrm{p}}$	+9.6°
West Subtropical Dominant (N=53)	44.0°N	122.1°W	–0.8°$^{\mathrm{p}}$	+15.1°

TABLE 1. Average characteristics of jet superposition events as a function of event type. These characteristics include the average starting latitude and longitude at which jet superpositions develop for each event type, and the average change (Δ) in latitude and longitude of a jet superposition centroid during the life span of each event type. Average changes in latitude or longitude that are statistically different from polar dominant events (“p”), hybrid events (“h”), subtropical dominant events (“s”), eastern subtropical dominant events (“e”), and/or western subtropical dominant events (“w”) at the 99% confidence level according to a two-sided Welch’s *t*-test are indicated with a superscript.

Figures

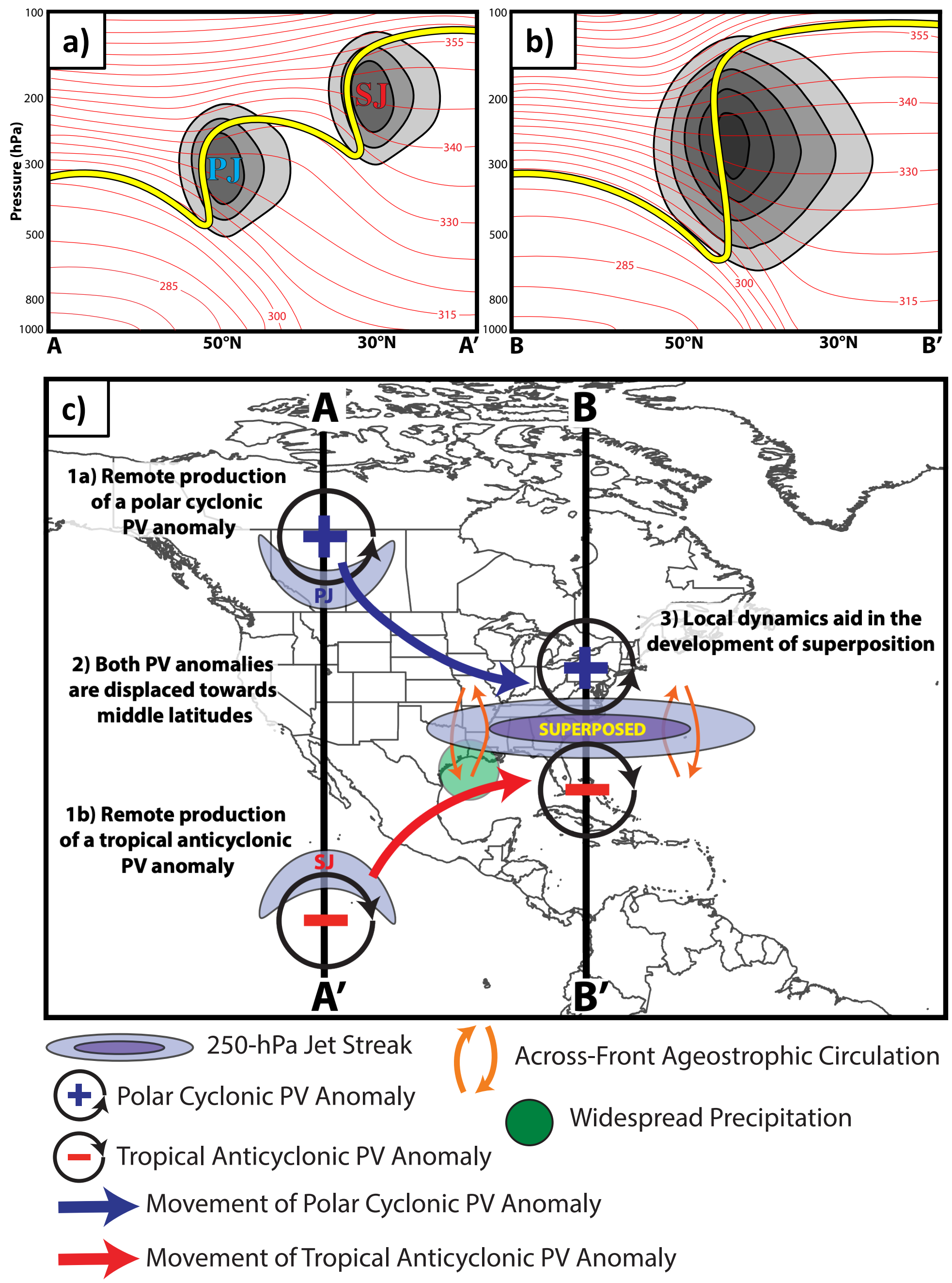

FIG. 1. (a) Idealized cross section along A–A′, as indicated in (c), through separate polar and subtropical jets. Wind speed (gray shading with darker shades of gray identifying stronger wind speeds), potential temperature (red lines every 5 K), and the 2-PVU contour (thick yellow line). The polar jet (PJ) and subtropical jet (SJ) are labeled accordingly. (b) As in (a), but for an idealized cross section along B–B′, as indicated in (c), through a jet superposition. (c) Conceptual model summarizing the development of a jet superposition. The locations of the polar jet (PJ), subtropical jet (SJ), and superposed jet are labeled accordingly. Figure and caption adapted from Winters and Martin (2017; their Fig. 2).

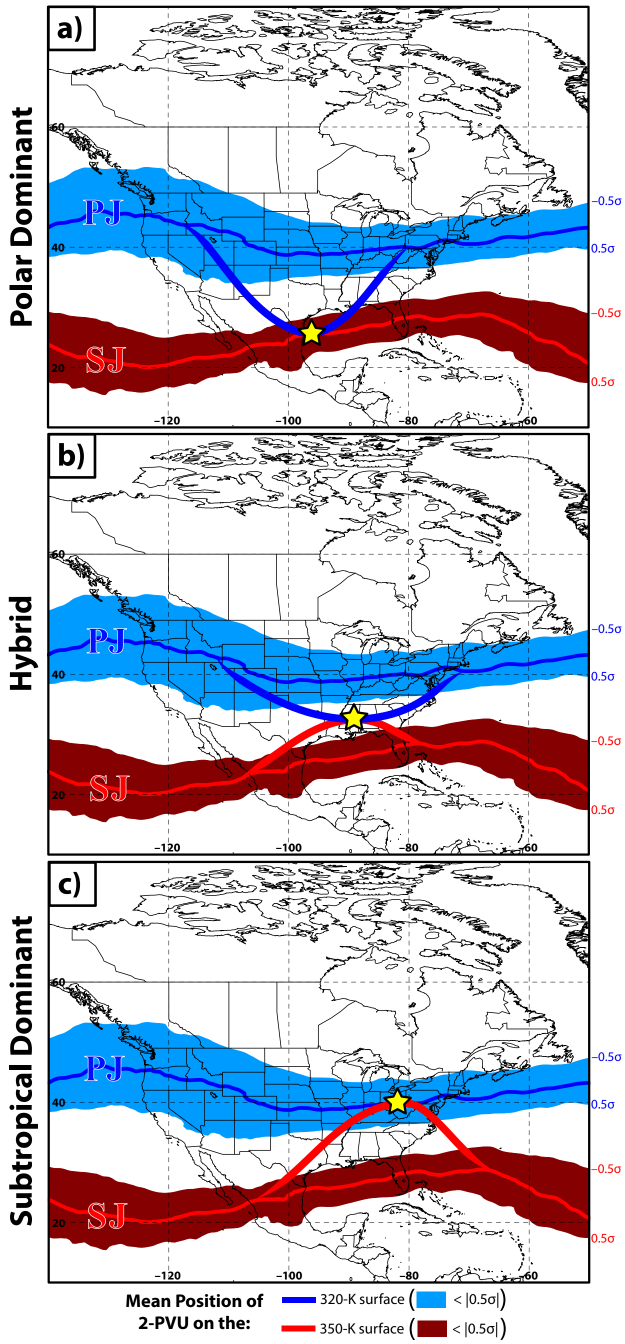

FIG. 2. The mean position of the 2-PVU contour on the 320-K and 350-K surfaces at 0000 UTC 1 January is indicated by the thin blue and red line, respectively, as a proxy for the position of the polar (PJ) and subtropical (SJ) waveguide. Shaded areas bounding each mean 2-PVU contour indicate locations at which an observation of 2-PVU on that particular isentropic surface would represent a standardized PV anomaly with an absolute magnitude less than 0.5. Hypothetical deviations of the 2-PVU contour from its mean position on each isentropic surface that result in the formation of (a) a polar dominant jet superposition event (yellow star) are indicated by the thick blue and red contours. (b) As in (a), but for a hybrid event. (c) As in (a), but for a subtropical dominant event.

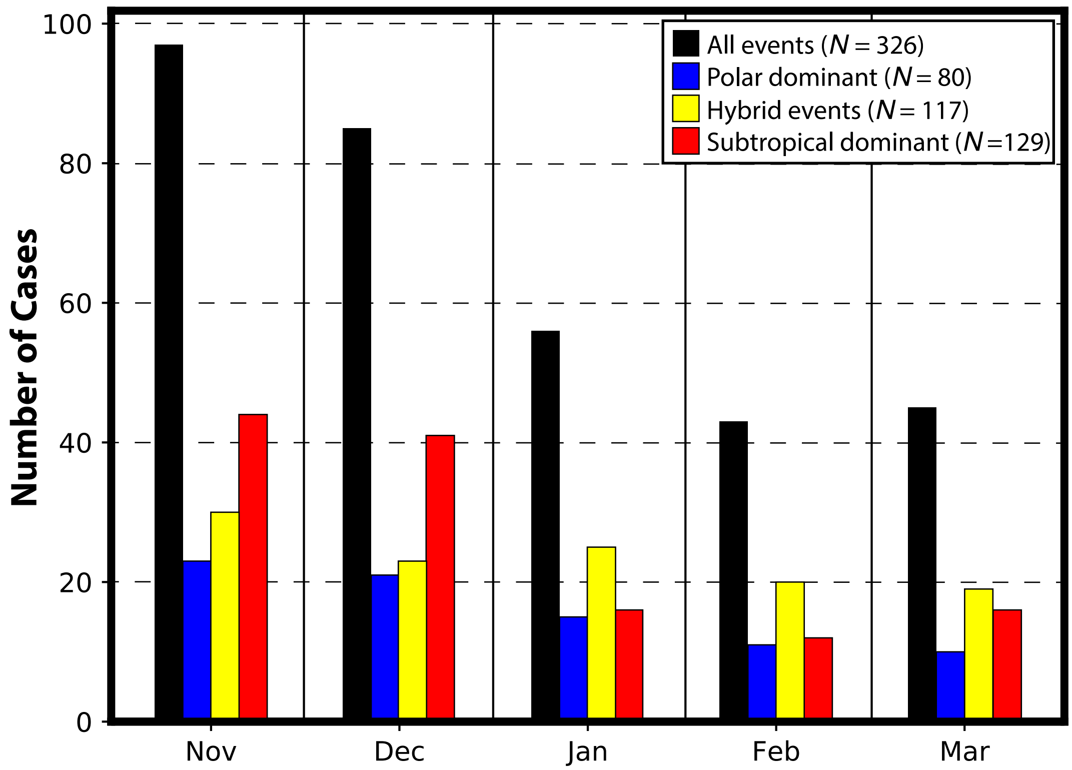

FIG. 3. Monthly frequency of jet superposition events as a function of event type.

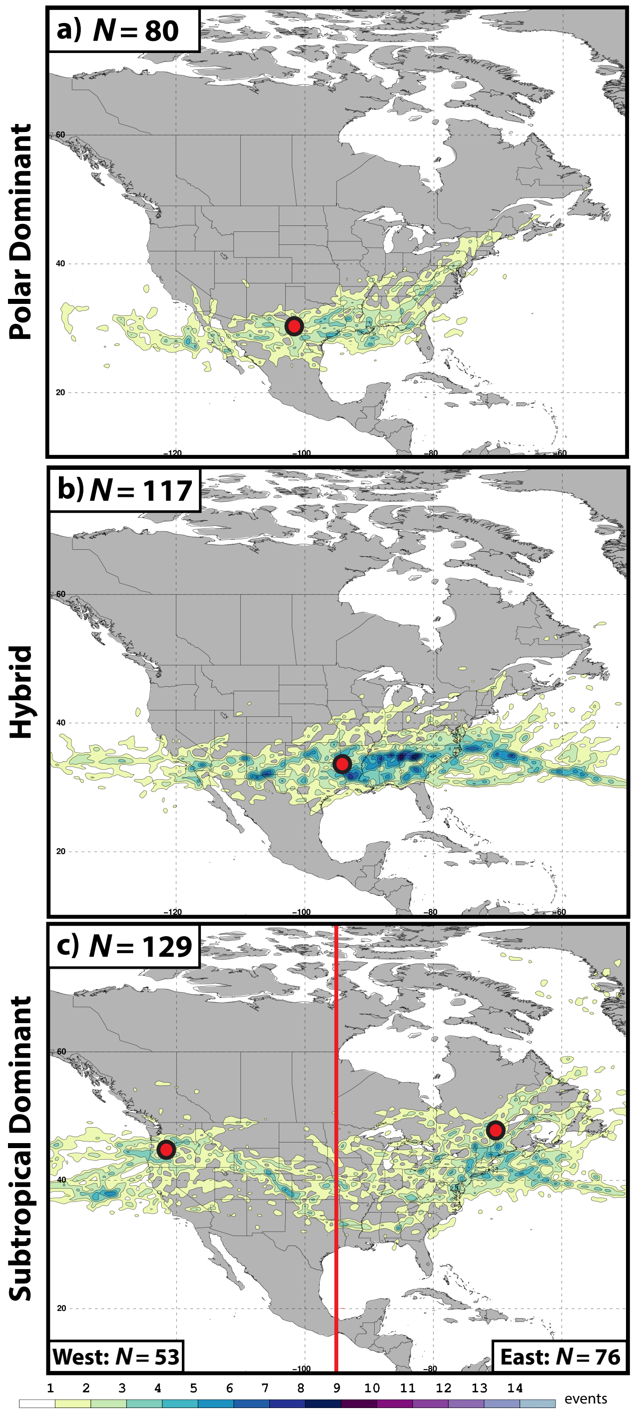

FIG. 4. (a) The frequency of polar dominant jet superposition events at each grid point is shaded according to the legend. The red circle represents the average starting latitude and longitude for polar dominant events. (b) As in (a), but for hybrid events. (c) As in (a), but for subtropical dominant events. The vertical red bar in (c) illustrates the partition of subtropical dominant events into an eastern and a western category. The red dots to the east and west of the vertical red line in (c) indicate the average location of superposition for eastern and western subtropical dominant events, respectively.

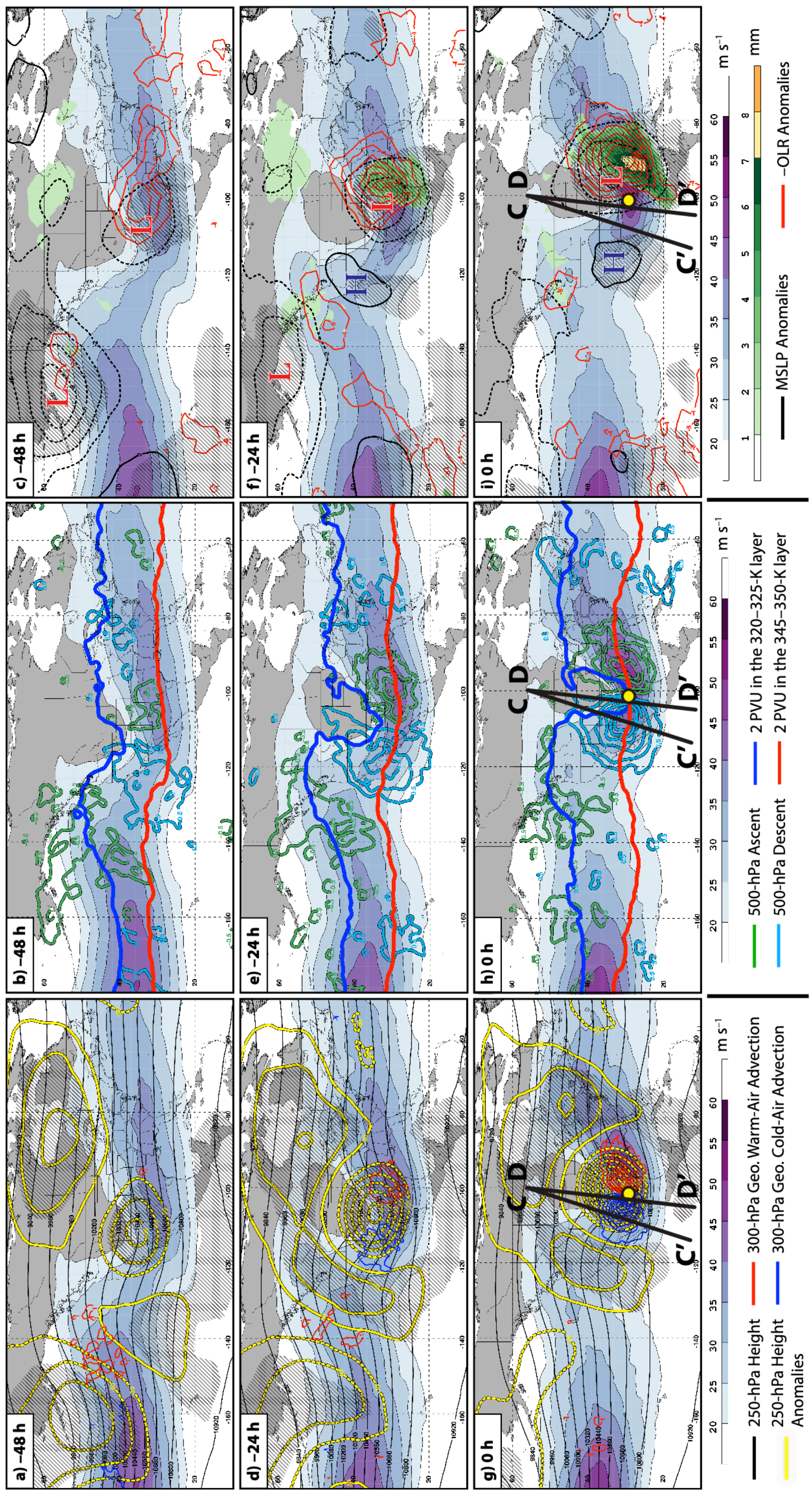
a) −48 h
b) −48 h
c) −48 h
d) −24 h
e) −24 h
f) −24 h
g) 0 h
h) 0 h
i) 0 h
C
D
C′
D′
250-hPa Height
250-hPa Height Anomalies
300-hPa Geo. Warm-Air Advection
300-hPa Geo. Cold-Air Advection
500-hPa Ascent
500-hPa Descent
2 PVU in the 320–325-K layer
2 PVU in the 345–350-K layer
MSLP Anomalies
−OLR Anomalies
m s⁻¹
mm

FIG. 5. Composite large-scale flow evolution prior to the initiation of a polar dominant jet superposition event. (left) 250-hPa geopotential height (black solid lines every 120 m), 250-hPa geopotential height anomalies (yellow lines every 30 m, solid when positive and dashed when negative), 250-hPa wind speed (shaded according to the legend in m s^{-1}), and 300-hPa geostrophic temperature advection (blue and red lines every 1×10^{-4} K s^{-1} for cold- and warm-air advection, respectively) for (a) 48 h, (d) 24 h, and (g) 0 h prior to jet superposition. Hatched areas represent locations where the 250-hPa geopotential height anomalies are statistically distinct from climatology at the 99% confidence level. (middle) 250-hPa wind speed (shaded according to the legend in m s^{-1}), the position of the 2-PVU contour within the 320–325-K and the 345–350-K layer is indicated by the thick blue and red line, respectively, as a proxy for the location of the polar and subtropical waveguide, and 500-hPa vertical motion (contoured every 0.5 dPa s^{-1} in green for ascent and in blue for descent) for (b) 48 h, (e) 24 h, and (h) 0 h prior to jet superposition. (right) 250-hPa wind speed (shaded according to the legend in m s^{-1}), mean sea level pressure anomalies (black lines every 2 hPa, solid when positive and dashed when negative), negative OLR anomalies (red lines every 4 W m^{-2}), and precipitable water anomalies (shaded according to the legend in mm at locations in which the anomalies are statistically distinct from climatology at the 99% confidence level) for (c) 48 h, (f) 24 h, and (i) 0 h prior to jet superposition. Hatched areas represent locations where the mean sea level pressure anomalies are statistically distinct from climatology at the 99% confidence level. The red "L"s and blue "H"s identify the locations of surface cyclones and anticyclones. The yellow dot in (g), (h), and (i) corresponds to the average location of jet superposition, and the vertical cross sections, C–C′ and D–D′, in (g), (h), and (i) are examined further in Figs. 7a,b, respectively.

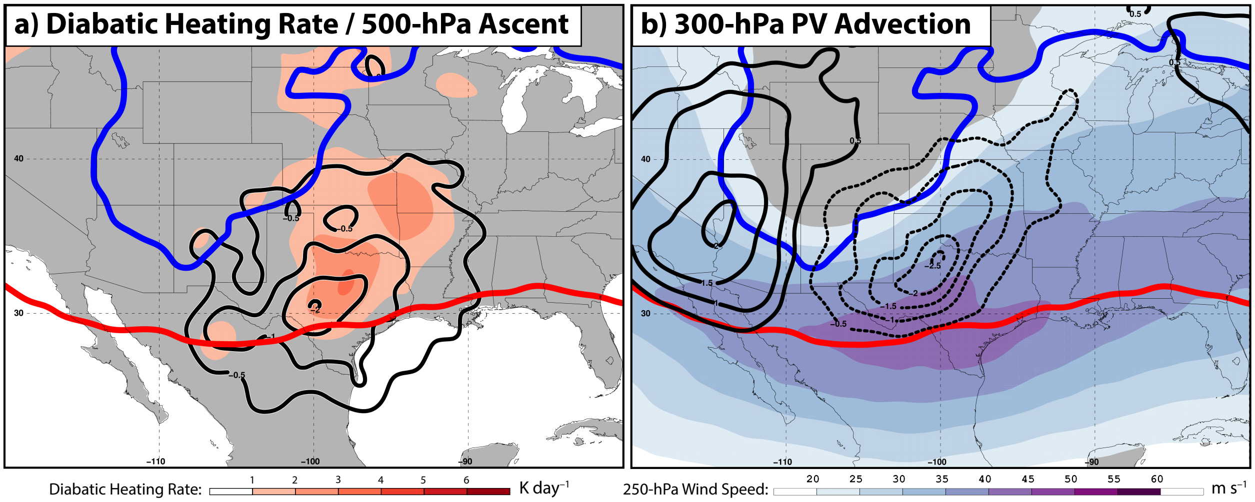

FIG. 6. (a) The diabatic heating rate (shaded according to the legend in K day^{-1}), 500-hPa ascent (black lines every –0.5 dPa s^{-1}), and the position of the 2-PVU contour within the 320–325-K and the 345–350-K layer is indicated by the thick blue and red line, respectively, 24-h prior to a polar dominant jet superposition. (b) As in (a), but with 250-hPa wind speed (shaded according to the legend in m s^{-1}), and 300-hPa PV advection by the three-dimensional divergent circulation (black contours every 0.5 × 10^{-5} PVU s^{-1}, solid when positive and dashed when negative).

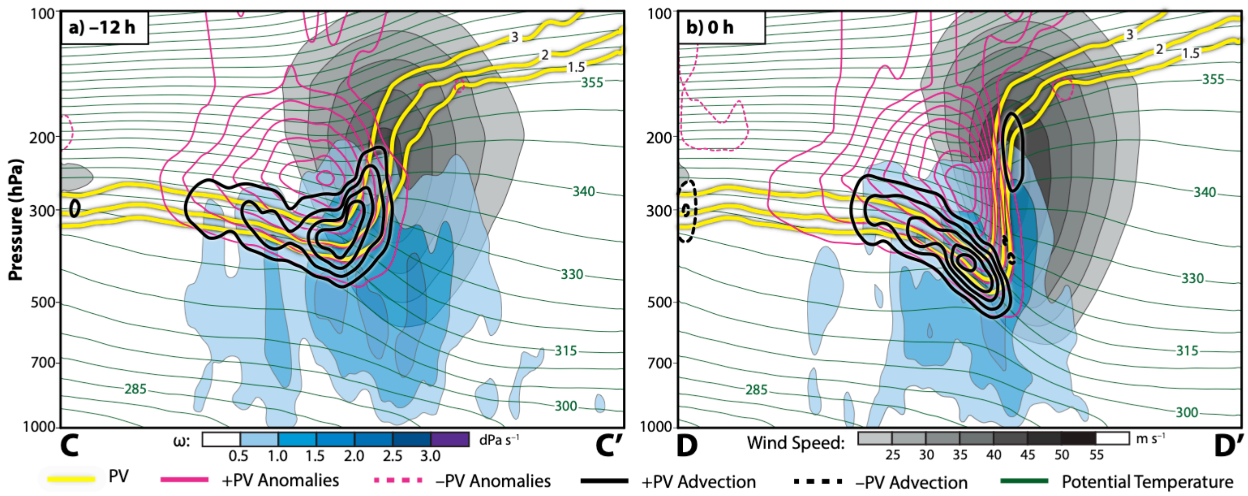

FIG. 7. (a) Cross section along C–C′, as indicated in Figs. 5g–i, 12 h prior to a polar dominant jet superposition. Potential temperature (green lines every 5 K), wind speed (gray shading according to the legend in m s^{-1}), PV anomalies (magenta lines every 0.5 PVU, solid when positive and dashed when negative), the 1.5-, 2-, and 3-PVU contours (yellow lines), PV advection by the three-dimensional divergent circulation (black lines every 0.5×10^{-5} PVU s^{-1}, solid when positive and dashed when negative), and descent (blue shading according to the legend in dPa s^{-1}). (b) As in (a), but for the cross section along D–D′, as indicated in Figs. 5g–i, 0 h prior to a polar dominant jet superposition event.

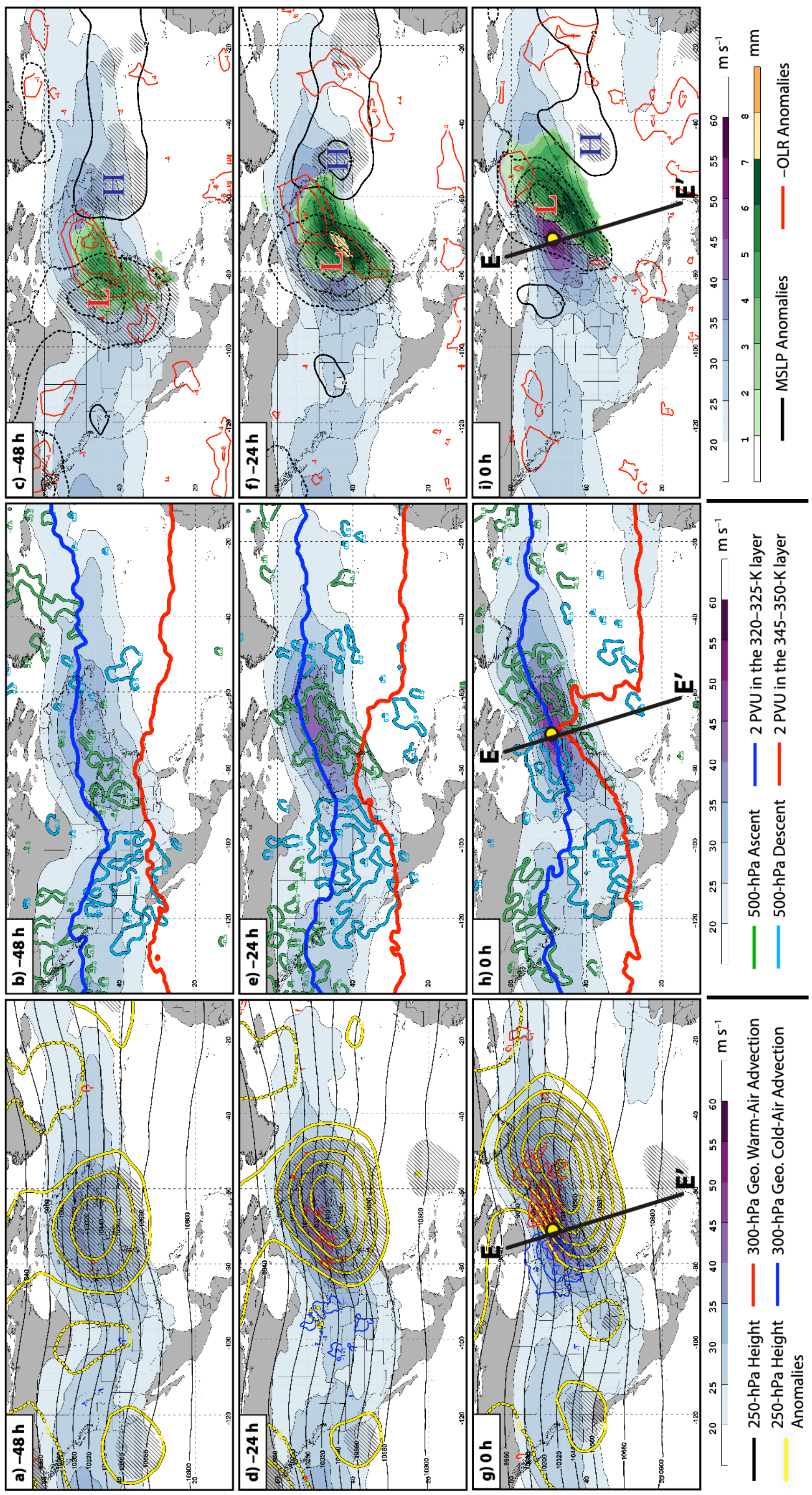

FIG. 8. Composite large-scale flow evolution prior to the initiation of an eastern subtropical dominant jet superposition event. All conventions are identical to those in Fig. 5.

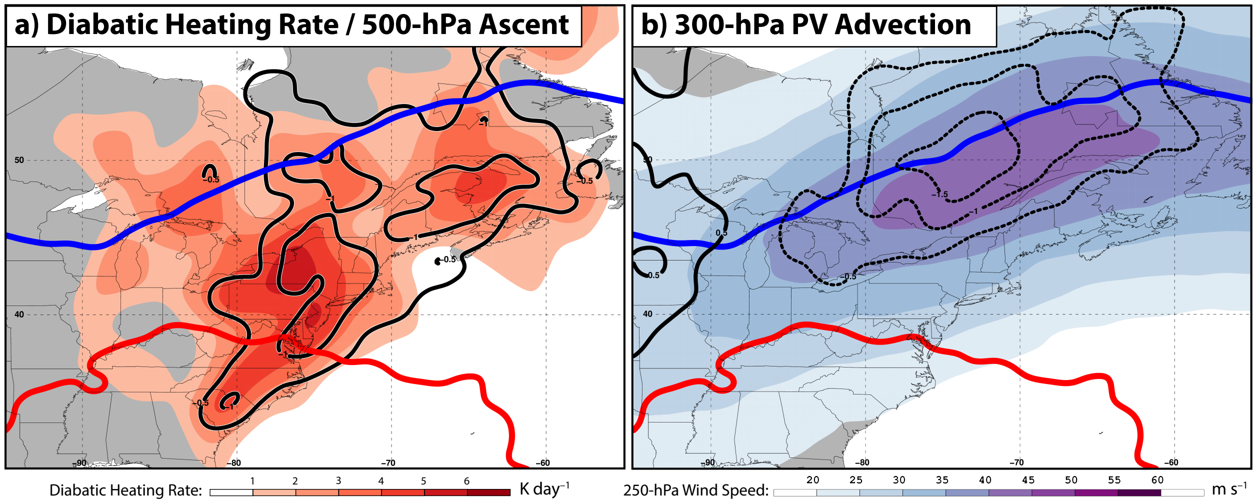

FIG. 9. As in Fig. 6, but for 24 h prior to an eastern subtropical dominant jet superposition event.

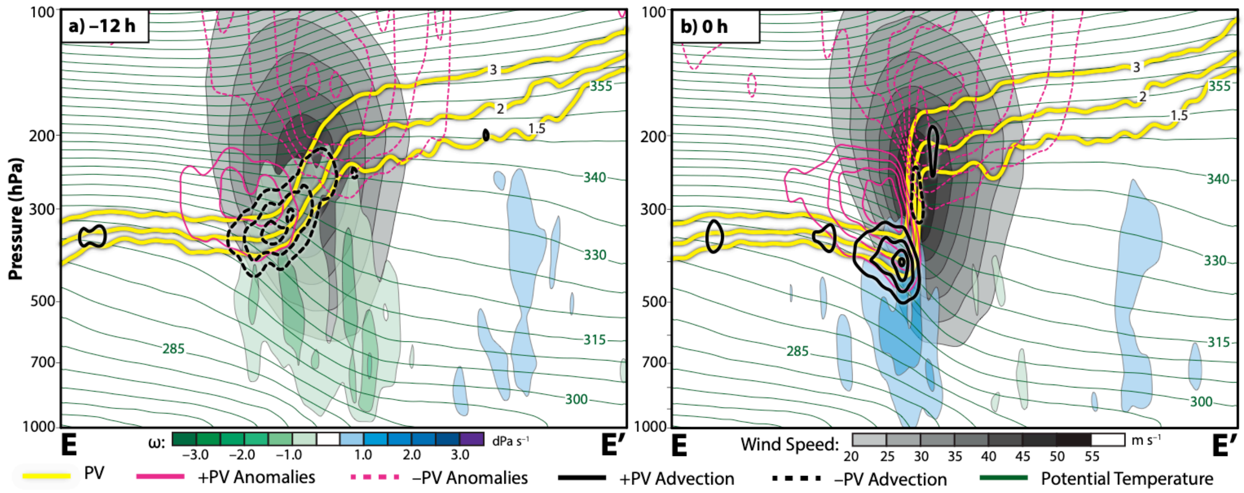

FIG. 10. (a) Cross section along E–E′, as indicated in Figs. 8g–i, 12 h prior to an eastern dominant jet superposition. All conventions are identical to those in Fig. 7, with the exception that ascent and descent are shaded in green and blue, respectively, according to the legend in dPa s^{-1}. (b) As in (a), but for 0 h prior to an eastern subtropical dominant jet superposition.

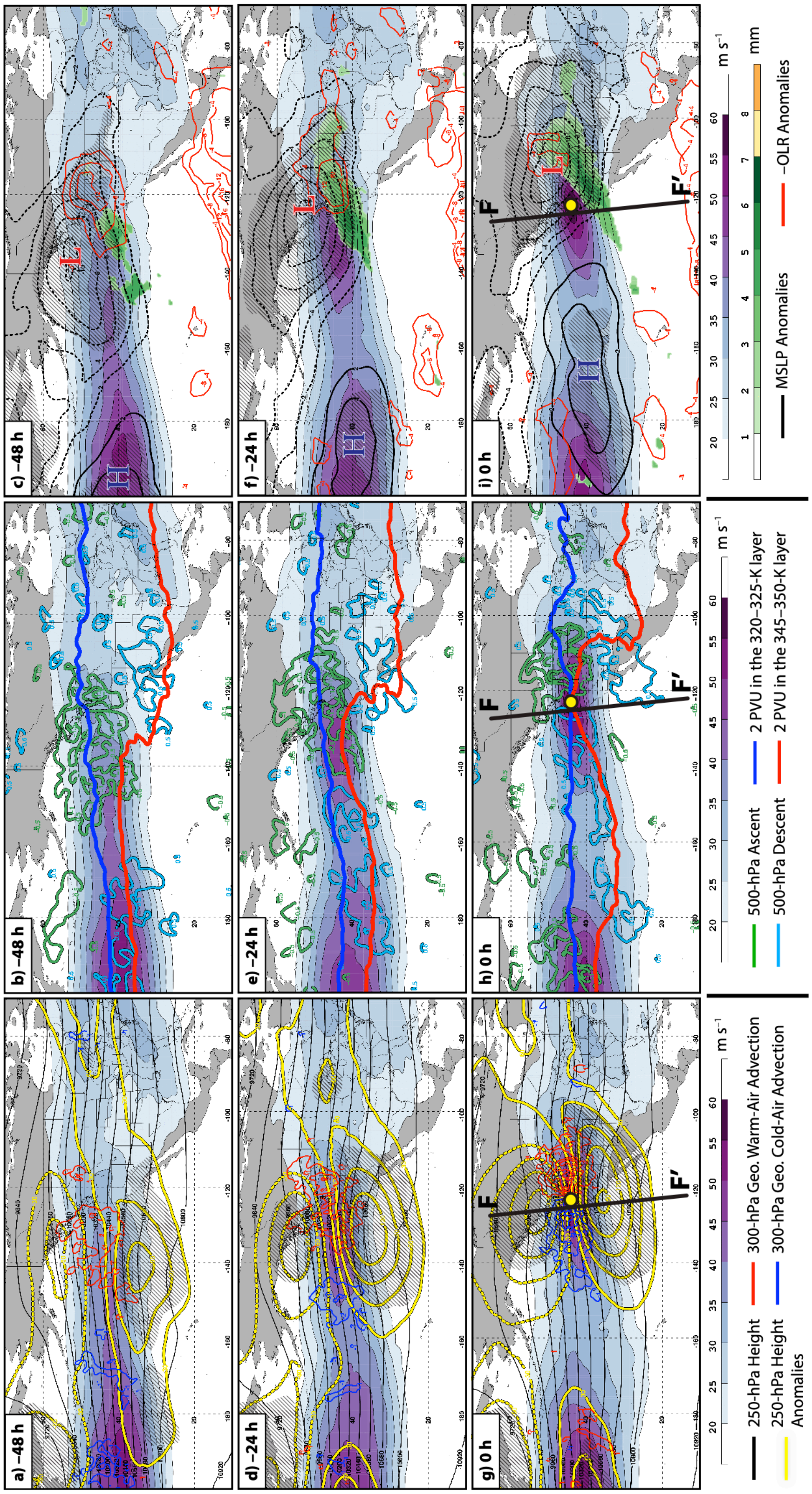

FIG. 11. Composite large-scale flow evolution prior to the initiation of a western subtropical dominant jet superposition event. All conventions are identical to those in Fig. 5.

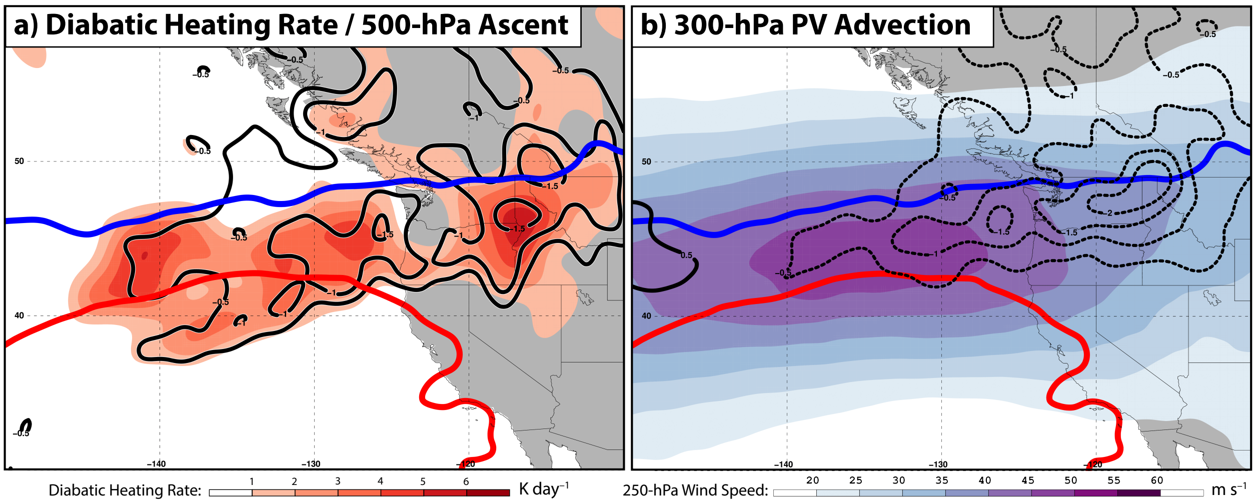

FIG. 12. As in Fig. 6, but for 24 h prior to a western subtropical dominant jet superposition event.

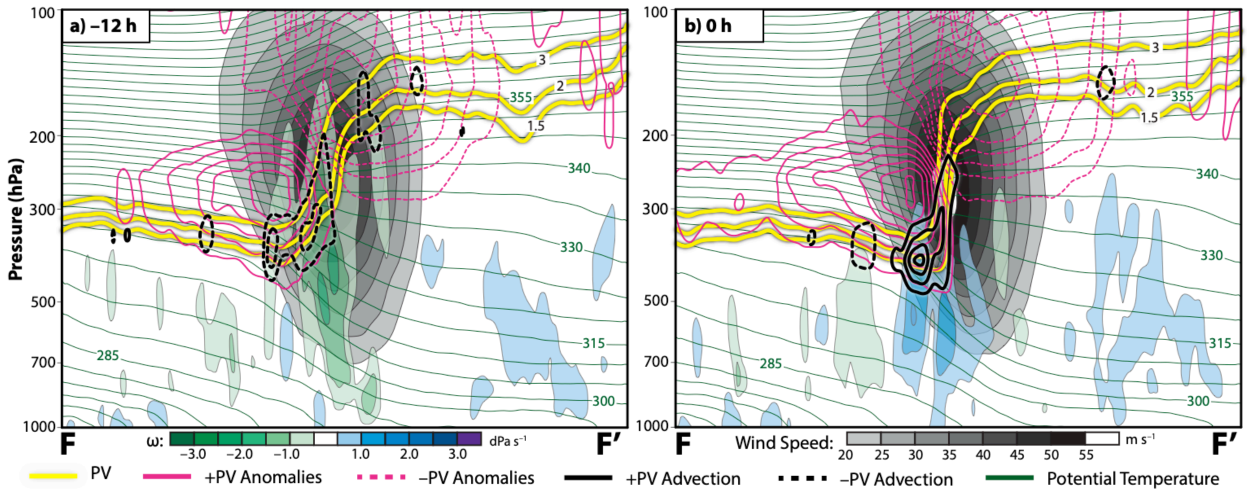

FIG. 13. (a) Cross section along F–F′, as indicated in Figs. 11g–i, 12 h prior to a western subtropical dominant jet superposition event. All conventions are identical to those in Fig. 10. (b) As in (a), but for 0 h prior to a western subtropical dominant jet superposition event.

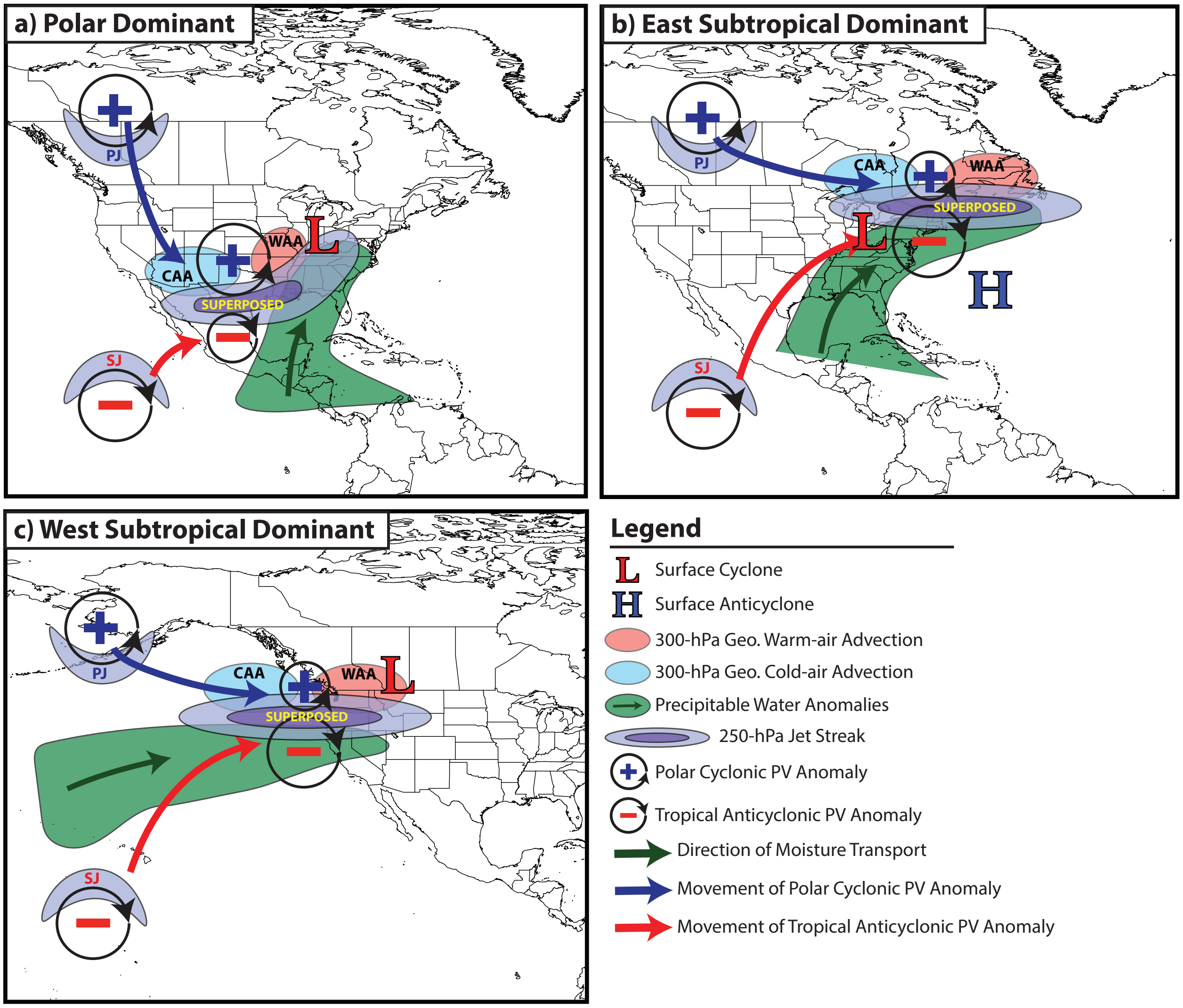

FIG. 14. Conceptual models for the development of (a) polar dominant, (b) eastern subtropical dominant, and (c) western subtropical dominant jet superposition events.